Structural Aspects, IR Study, and Molecular Photophysics of the Cumulene-Bridged Complexes with Rhenium(I), Ruthenium(II), and Osmium(II) Centers

Jeffrey V. Ortega,[†] Kay Khin, Wytze E. van der Veer, Joseph Ziller, and Bo Hong*

Department of Chemistry, University of California, Irvine, California 92697-2025

Received June 23, 2000

The synthesis of a series of Re^{I}, Ru^{II}, and Os^{II} complexes that contain rigid polyphosphine/cumulene spacers is reported here. These cumulenic ligands, namely, 1,1′,3,3′-tetrakis(diphenylphosphino)allene (**C_3P_4**) and 1,1′,4,4′-tetrakis(diphenylphosphino)cumulene (**C_4P_4**), utilize diphenylphosphino linkage components to coordinate to the metal−polypyridyl or metal−carbonyl units. Characterization of all mono-, homo-, and heterobimetallic complexes is achieved using $^{31}P\{^{1}H\}$ NMR, IR, and fast atom bombardment mass spectroscopy (FAB/MS) and elemental analysis. The two Re^{I} homobimetallic complexes were also characterized by single-crystal X-ray structure determination, which provided the structural evidence of a 90° rotation between the C_3 and C_4 adducts causing a change in the electrochemical behavior. The ground-state electronic absorption and redox interactions, along with the excited-state photophysical characteristics, are also explored. Electrochemical studies showed that an increase in the carbon chain length resulted in a greater amount of σ-donation from the ligand to the metal centers, as well as a greater amount of electronic communication between the metal termini of the bimetallic species. The electronic absorption and emission spectra of the new complexes were also determined and characterized. The lifetimes of the excited-state luminescence of the Re^{I} mono- and homobimetallic complexes were found to be an order of magnitude shorter than the lifetimes of the heterobimetallic complexes containing the Ru^{II} and Os^{II} moieties. Excited-state energy transfer was observed from the higher MLCT excited state of the Re^{I} centers to the lower energy MLCT excited state of the Ru^{II} and Os^{II} centers on the following basis: no Re^{I}-based emission was detected in the steady-state emission measurements, the time-resolved decay traces were fitted to only single-exponential decays, and the quantum yields were identical for each compound at two different excitation wavelengths where different percentages of the metal-based chromophores were excited.

Introduction

The combination of metal-based units with rigid organic spacers constitutes a fundamental class of functional supramolecular systems, namely, "molecular wires" or rigid rodlike molecules.[1−10] With the incorporation of redox-active and photoactive metal-based chromophores, functional supramolecular systems can be constructed, and their redox characteristics, excited-state properties, and signal transport processes can be fine-tuned and investigated. To achieve this, the spacers utilized must have desired characteristics such as rigidity, photostability, and molecular orbitals with suitable energies to overlap with those of the tethered metal units.[1,4−6] Under the appropriate conditions, the degree of interaction between the

* To whom all correspondence should be addressed.

[†] Currently at Department of Chemistry, Northwestern University, Evanston, IL.

(1) (a) Falloon, S. B.; Szafert, S.; Arif, A. M.; Gladysz, J. A. *Chem. Eur. J.* **1998**, *4*, 1033−1042. (b) Weng, W. Q.; Bartik, T.; Brady, M.; Bartik, B.; Ramsden, J. A.; Arif, A. M.; Gladysz, J. A. *J. Am. Chem. Soc.* **1995**, *117*, 11922−11931. (c) Bartik, B.; Dembinski, R.; Bartik, T.; Arif, A. M.; Gladysz, J. A. *New J. Chem.* **1997**, *21*, 739−750. (d) Falloon, S. B.; Weng, W. Q.; Arif, A. M.; Gladysz, J. A. *Organometallics* **1997**, *16*, 2008−2015. (e) Brady, M.; Weng, W. Q.; Zhou, Y. L.; Seyler, J. W.; Amoroso, A. J.; Arif, A. M.; Bohme, M.; Frenking, G.; Gladysz, J. A. *J. Am. Chem. Soc.* **1997**, *119*, 775−788. (f) Brady, M.; Weng, W. Q.; Gladysz, J. A. *J. Chem. Soc., Chem. Commun.* **1994**, 2655−2656. (g) Falloon, S. B.; Arif, A. M.; Gladysz, J. A. *Chem. Commun.* **1997**, 629−630. (h) Bartik, T.; Bartik, B.; Brady, M.; Dembinski, R.; Gladysz, J. A. *Angew. Chem., Int. Ed. Engl.* **1996**, *35*, 414−417.

(2) Mayr, A.; Yu, M. P. Y.; Yam, V. W. W. *J. Am. Chem. Soc.* **1999**, *121*, 1760−1761.

(3) (a) Ortega, J. V.; Hong, B.; Ghosal, S.; Hemminger, J. C.; Breedlove, B.; Kubiak, C. P. *Inorg. Chem.* **1999**, *38*, 5102−5112. (b) Hong, B.; Woodcock, S. R.; Saito, S. K.; Ortega, J. V. *J. Chem. Soc., Dalton Trans.* **1998**, 2615−2623. (c) Hong, B.; Ortega, J. V. *Angew. Chem., Int. Ed.* **1998**, *37*, 2131−2134.

(4) (a) Benniston, A. C.; Harriman, A.; Grosshenny, V.; Ziessel, R. *New J. Chem.* **1997**, *21*, 405−408. (b) Grosshenny, V.; Harriman, A.; Ziessel, R. *Angew. Chem., Int. Ed. Engl.* **1995**, *34*, 2705−2708. (c) Benniston, A. C.; Grosshenny, V.; Harriman, A.; Ziessel, R. *Angew. Chem., Int. Ed. Engl.* **1994**, *33*, 1884−1885. (d) Grosshenny, V.; Ziessel, R. *J. Chem. Soc., Dalton Trans.* **1993**, 817−819. (e) Ziessel, R.; Juris, A.; Venturi, M. *Inorg. Chem.* **1998**, *37*, 5061−5069. (f) Harriman, A.; Ziessel, R. *Chem. Commun.* **1996**, 1707−1716. (g) Grosshenny, V.; Harriman, A.; Gisselbrecht, J. P.; Ziessel, R. *J. Am. Chem. Soc.* **1996**, *118*, 10315−10316. (h) Grosshenny, V.; Harriman, A.; Ziessel, R. *Angew. Chem., Int. Ed. Engl.* **1995**, *34*, 1100−1102.

(5) Bunz, U. H. F. *Angew. Chem., Int. Ed. Engl.* **1996**, *35*, 969−971.

(6) Hong, B. *Comments Inorg. Chem.* **1999**, *20*, 177−207.

(7) (a) Coat, F.; Guillevic, M. A.; Toupet, L.; Paul, F.; Lapinte, C. *Organometallics* **1997**, *16*, 5988−5998. (b) Guillemot, M.; Toupet, L.; Lapinte, C. *Organometallics* **1998**, *17*, 1928−1930. (c) Le Narvor, N.; Toupet, L.; Lapinte, C. *J. Am. Chem. Soc.* **1995**, *117*, 7129−7138. (d) Le Narvor, N.; Lapinte, C. *J. Chem. Soc., Chem. Commun.* **1993**, 357−359. (e) Coat, F.; Lapinte, C. *Organometallics* **1996**, *15*, 477−479.

(8) Woodworth, B. E.; White, P. S.; Templeton, J. L. *J. Am. Chem. Soc.* **1997**, *119*, 828−829.

(9) (a) El-ghayoury, A.; Harriman, A.; Khatyr, A.; Ziessel, R. *Angew. Chem., Int. Ed.* **2000**, *39*, 185−189. (b) Harriman, A.; Ziessel, R. *Coord. Chem. Rev.* **1998**, *171*, 331−339. (c) Ziessel, R.; Hissler, M.; El-Ghayoury, A.; Harriman, A. *Coord. Chem. Rev.* **1998**, *180*, 1251−1298.

(10) (a) Derege, P. J. F.; Therien, M. J. *Inorg. Chim. Acta* **1996**, *242*, 211−218. (b) Lin, V. S. Y.; Therien, M. J. *Chem. Eur. J.* **1995**, *1*, 645−651.

10.1021/ic0006910 CCC: $19.00
Published on Web 12/01/2000

metal termini can be probed by studying parameters such as the rate of photoinduced energy/electron transfer, the electronic coupling matrix element (H_{AB}), and the comproportionation constant (K_c). These rigid rodlike molecules may serve as media to explore the basic properties that govern the fundamental aspects of electronic communication and photophysical characteristics in molecular systems.

Specifically, the linear, one-dimensional forms of carbon have attracted growing interest as suitable molecular building blocks for the construction of supramolecular systems, especially the rigid rodlike molecules.[1−5] These carbon chains can exist as sp-hybridized carbon atoms either in an uninterrupted series of double bonds (cumulenes) or as alternating triple and single bonds (polyynes). They can serve as passive bridging component or active conduit for signal transport between various combinations of metal-based moieties. The unsaturation can cause these carbon chains to exhibit extraordinary properties.[1c−d,4b] Such properties are manifested in the rigid molecule's ability to convey electrons efficiently from one end to the other as well as the capability of unidirectional electron/energy transfer. In addition, by "capping" the rigid molecular rods with photoactive and redox-active metal-based units, it is then possible to study the electronic, optical, and electrochemical interactions between two linked organometallic centers.[1e,f,3,4c−d,6] These metal-capped carbon chains are of great interest due to their potentially useful materials properties. Conjugated carbon rods are expected to have a high degree of mechanical strength and stability, which is important for making robust and resilient materials.[5] Their expected electrical conductivity could lead to applications such as "molecular wires" in electronic devices.[1g,4b−h,5] This property would also render them useful for studying how charge is transported from one metal-based moiety to another over a long molecular distance.

Several laboratories have focused on the development of one-dimensional molecular wires. For the majority of the research in this area, the focus of the investigation has been primarily on the acetylenic form of sp carbon chains.[1,2,4−11] Lapinte and co-workers have bridged two iron centers by an elemental four-carbon chain[7a−d] and an eight-carbon chain[7e] consisting of sp-hybridized polyynes that both facilitated a strong coupling between Fe^{II}/Fe^{II} and Fe^{II}/Fe^{III} centers. Gladysz and co-workers[1h] have synthesized systems with rigid acetylenic carbon chains between metal centers and a chain length as long as 20 carbons. Gladysz[11] has also developed a system *in situ* that contained a cumulenic five-carbon rigid spacer that acted as a Fischer carbene and facilitated the charge transfer from Re^{I} to Mn^{I}. Templeton and co-workers[8] have bridged molybdenum and tungsten tris(pyrazolyl)borate carbonyl units by a C_4 cumulenic carbon chain that converted into an acetylenic bridge with metal−carbon triple bonds. In those complexes, the coordination site is the C_n chain itself, where the terminal carbon atoms are bonded directly to the metal centers. However, no excited-state properties have been reported for such systems.

Other types of linkage components have been incorporated to couple the rigid acetylenic bridge with metal centers. Harriman and Ziessel[9] have utilized polypyridyl units connected to alkyne bridges to coordinate to metal centers. Specifically, both terpyridyl and bipyridyl groups were used in conjunction with C_2 and C_4 acetylenic units. This combination of π-conjugated acetylenic groups with the aryl polypyridyl groups has resulted in the facilitation of rapid intramolecular energy transfer. Porphyrins have also been combined with rigid acetylenic chains by Therien and co-workers to coordinate with different metal centers.[10] These are examples describing the versatility that can be engineered with the utilization of different coordination or linkage units.

Recently our group has become interested in the development of rigid rodlike systems with Re^{I}, Ru^{II}, and Os^{II} termini and ditopic/tetratopic polyphosphines with cumulenic and acetylenic carbon chains. Herein, we report the synthesis, X-ray structure determination, redox characteristics, and photophysical studies of a new family of monometallic (**ReC$_n$P$_4$**, n = 3, 4), homobimetallic (**ReC$_n$P$_4$Re**), and heterobimetallic species (**ReC$_n$P$_4$M**, M = Ru, Os) with Re^{I}, Ru^{II}, and/or Os^{II} centers. The polyphosphine spacers, namely, 1,1′,3,3′-tetrakis(diphenylphosphino)allene (**C$_3$P$_4$**) and 1,1′,4,4′-tetrakis(diphenylphosphino) cumulene (**C$_4$P$_4$**), are used to link together the metal centers. The sp-hybridized carbon chains in the spacers not only control the conformational rigidity of the overall complex but also determine the planarity and the distance between the two terminal units. The mono-, homo-, and heterobimetallic complexes with only the Ru^{II} and/or Os^{II} centers were described elsewhere.[3,6] In this study, we report the first structural evidence of a 90° rotation between the Re^{I} homobimetallic C_3 and C_4 adducts that were initially demonstrated by the electrochemical studies of the homobimetallic Ru^{II} and Os^{II} adducts. The redox chemistry and excited-state properties are discussed and compared with the analogous monometallic species as well as the model complex containing 1,1′-bis(diphenylphosphino)ethene (**C$_2$P$_2$e**). Other characterization techniques, including infrared spectroscopy (IR), $^{31}P\{^{1}H\}$ nuclear magnetic resonance (NMR) spectroscopy, fast atom bombardment mass spectroscopy (FAB/MS), and elemental analysis (EA), were also used to structurally characterize all new complexes. In addition, the ground-state electronic absorption properties, the excited-state decay kinetics, and the energy transfer process (using Re^{I}/Ru^{II} and Re^{I}/Os^{II} donor/acceptor pairs) are also explored in this system with short sp carbon chains.

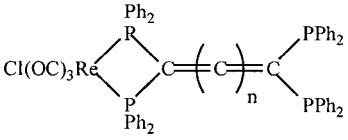

n = 1, **ReC$_3$P$_4$**; 2, **ReC$_4$P$_4$**

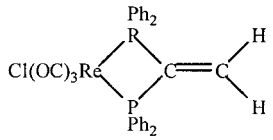

ReC$_2$P$_2$e

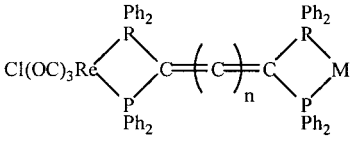

M = Re(CO)$_3$Cl; n = 1, **ReC$_3$P$_4$Re**; 2, **ReC$_4$P$_4$Re**
M = Ru(bpy)$_2$; n = 1, **RuC$_3$P$_4$Re**; 2, **RuC$_4$P$_4$Re**
M = Os(bpy)$_2$; n = 1, **OsC$_3$P$_4$Re**; 2, **OsC$_4$P$_4$Re**

Experimental Section

General Methods. All experiments were carried out under a nitrogen atmosphere using standard glovebox and Schlenk techniques. All purifications by column chromatography were performed in the absence of light using basic alumina and either $CHCl_3$ or MeCN as eluent. The monometallic species were collected as the first fraction, while the bimetallic complexes were collected as the second fraction.

(11) (a) Weng, W. G.; Bartik, T.; Gladysz, J. A. *Angew. Chem., Int. Ed. Engl.* **1994**, *33*, 2199−2202. (b) Bartik, T.; Weng, W. Q.; Ramsden, J. A.; Szafert, S.; Falloon, S. B.; Arif, A. M.; Gladysz, J. A. *J. Am. Chem. Soc.* **1998**, *120*, 11071−11081.

Materials. 1,1′,3,3′-Tetrakis(diphenylphosphino)allene (**C_3P_4**),[12a] 1,1′,4,4′-tetrakis(diphenylphosphino)cumulene (**C_4P_4**),[12b] 1,1′-bis(diphenylphosphino)ethene (**C_2P_2e**),[12c] and *cis*-$Os(bpy)_2Cl_2$[13] were prepared according to literature methods. $[(bpy)_2M(C_nP_4)](PF_6)_2$ (M = Ru, Os; n = 3, 4) were synthesized as previously described.[3] *cis*-$Ru(bpy)_2Cl_2$ and $Re(CO)_5Cl$ were purchased from Strem and used as received. All spectroscopic grade solvents were purchased from Fisher and used without further purification. Tetrahydrofuran (THF) was distilled under nitrogen over sodium benzophenone ketyl. Acetonitrile (MeCN) was distilled under nitrogen over calcium hydride.

Physical Measurements. Electrochemical Analysis. Cyclic voltammograms were recorded on a CHI 630 electrochemical analyzer. The redox behavior can be monitored in "dry" aprotic solvents that contain a supporting electrolyte. Typical experiments were run at 100 mV/s in acetonitrile with 0.1 M tetrabutylammonium hexafluorophosphate as the electrolyte. A Ag/AgCl wire was used as a pseudoreference electrode, a platinum wire as the counter electrode, and a 1.0 mm platinum disk electrode as the working electrode. Great care was taken to remove oxygen as well as water in order to ensure the quality of the measurements. A ferrocene standard was used to reference the observed potential vs SCE.

NMR, IR, and Mass Spectral Analysis. $^{31}P\{^1H\}$ NMR spectra were obtained either in acetone-d_6 or in acetonitrile-d_3 on an Omega 500 MHz spectrometer, referenced to an external standard solution of 85% H_3PO_4 in D_2O. Infrared absorption (IR) spectra (KBr pellets) were collected as the average of 16 scans by using a Nicolet Impact Model 410 FT-IR with a DTGS (dueterated triglyme sulfate) detector. Fast atom bombardment mass spectral analysis (FAB/MS) data were obtained on a Micromass (Altrincham, UK) Autospec mass spectrometer at the UC, Irvine Mass Spectral Laboratory. Cesium ions at 25 kV were the bombarding species, and the matrix was *meta*-nitro benzyl alcohol (mNBA).

Photophysical Measurements. The electronic absorption spectra were recorded on a Hewlett-Packard 8453 diode array spectrophotometer. Steady-state emission spectra were obtained on a Hitachi 4500 fluorescence spectrometer or an AMINCO-Bowman Series 2 luminescence spectrometer. Luminescence quantum yields of all complexes were measured in spectrograde acetonitrile relative to $[Ru(bpy)_3][PF_6]_2$ ($\Phi = 0.062$[14] in acetonitrile).

The time-resolved emission spectroscopic studies were performed on a nanosecond laser flash photolysis unit equipped with a Continuum Surelite II-10 Q-switched Nd:YAG laser and a Surelite OPO (optical parametric oscillator) tunable visible source, a LeCroy 9350A oscilloscope, and a Spex 270 MIT-2x-FIX high-performance scanning and imaging spectrometer. Only lifetimes longer than 6 ns were measured accurately on this setup. For lifetimes shorter than 6 ns, they were obtained on a SLM-Aminco 48000 MHF Fourier transform spectrofluorometer. As a light source, the 488 nm line of a Coherent Innova 90 argon ion laser was used. The laser beam was modulated with a comb function with an interval spacing of 5 MHz, with a maximum frequency of 250 MHz. The resulting beam was imaged on the sample; the resulting fluorescence was detected with a photomultiplier via a Schott filter (OG 515). The phase and intensity of each component of the comb function was determined; the required reference signal was obtained by the utilization of a small portion of the incident beam. The resulting signals were fitted with a single exponential, which obtained the best fit with respect to both the recorded phase and intensity information. For each sample a series of five measurements was obtained, each consisting of 1000 scans.

$Cl(CO)_3Re(C_2P_2e)$ (ReC_2P_2e). To a refluxing solution of $Re(CO)_5Cl$ (128.8 mg, 0.356 mmol) in THF (20 mL) was added dropwise a solution of **C_2P_2e** (155.1 mg, 0.392 mmol) in THF (10 mL) over 30 min. After stirring for 24 h at reflux, the reaction mixture was cooled to room temperature before the solvent was removed by rotary evaporation. The yellow product was extracted using MeCN. After the solvent was removed, the yield was quantitative. $^{31}P\{^1H\}$ NMR (202.5 MHz, benzene-d_6): δ −8.41 (s) ppm. FT-IR (KBr): ν_{CO} 2029 (vs), 1952 (vs), 1895 (vs) cm^{-1}. Anal. Calcd for $C_{29}H_{22}O_3P_2ClRe$: C, 49.61; H, 3.15. Found: C, 49.71; H, 3.10.

$Cl(CO)_3Re(C_3P_4)$ (ReC_3P_4). A solution of $Re(CO)_5Cl$ (60.7 mg, 0.168 mmol) in THF (10 mL) was added to a refluxing solution of **C_3P_4** (236.1 mg, 0.300 mmol) in THF (20 mL). After refluxing for 24 h, the reaction mixture was cooled to room temperature. The volume of the solution was reduced down to ∼2 mL before being added dropwise into a stirred solution of hexanes (50 mL). The resulting yellow precipitate was collected by filtration, washed with 3 × 15 mL of hexanes, and dried *in vacuo*. Purification was performed by column chromatography using basic alumina as the support and $CHCl_3$ as the eluent, and the product was collected as the first fraction. Yield: 124.4 mg (68.4%). $^{31}P\{^1H\}$ NMR (202.5 MHz, acetone-d_6): δ 22.80 (s), −13.30 (s) ppm. FT-IR (KBr): ν_{CO} 2026 (vs), 1944 (vs), 1991 (vs) cm^{-1}. Anal. Calcd for $C_{54}H_{40}O_3P_4ClRe$: C, 59.91; H, 3.72. Found: C, 59.75; H, 3.68.

$Cl(CO)_3Re(C_3P_4)Re(CO)_3Cl$ (ReC_3P_4Re). A solution containing both $Re(CO)_5Cl$ (48.0 mg, 0.132 mmol) and **C_3P_4** (50.0 mg, 0.064 mmol) in THF (20 mL) was heated at reflux 24 h. Upon completion, the solution was allowed to cool to room temperature, and the solvent reduced down to ∼2 mL with the use of a rotary evaporator. The 2 mL sample was added dropwise into a stirred solution of hexanes (50 mL). The resulting yellow precipitate was collected by filtration, washed with 3 × 15 mL of hexanes, and dried *in vacuo*. Purification was performed by column chromatography using basic alumina as the support and $CHCl_3$ as the eluent, and the product was collected as the second fraction. Crystals were obtained by first dissolving the yellow powder in a minimum amount of THF and then adding an equivalent amount of benzene. The solution mixture was stored at room temperature in a vented container. As the THF evaporated, yellow needles formed. Yield: 80.0 mg (87.3%). $^{31}P\{^1H\}$ NMR (202.5 MHz, acetone-d_6): δ −1.43 (d), −12.75 (d) ppm. ^{13}C NMR (125.7 MHz, acetone-d_6): δ 136.23 and 135.25 (d, J_{CP} = 11.3−12.6 Hz, phenyls C_i and C_i'), 134.47 and 131.44 (d, J_{CP} = 2.0 Hz, phenyls C_p and C_p'), 133.68 and 131.98 (d, J_{CP} = 12.6−13.9 Hz, =CP_2), 132.70 (dd, J_{CP} = 17.6 and 2.3 Hz, C=*C*=C), 130.15−129.68 (m, phenyls C_m, C_m', C_o, and C_o'). FT-IR (KBr): ν_{CO} 2026 (vs), 1946 (vs), 1914 (vs), 1878 (w) cm^{-1}. Anal. Calcd for $C_{57}H_{40}O_6P_4Cl_2Re_2$: C, 49.32; H, 2.90. Found: C, 49.33; H, 2.95.

$[(bpy)_2Ru(C_3P_4)Re(CO)_3Cl](PF_6)_2$ (RuC_3P_4Re). A solution containing both $Re(CO)_5Cl$ (15.0 mg, 0.042 mmol) and **RuC_3P_4** (42.2 mg, 0.029 mmol) in MeCN (20 mL) was heated at reflux for 48 h. Upon completion, the solution was allowed to cool to room temperature, and the solvent reduced down to ∼2 mL with the use of a rotary evaporator. The 2 mL sample was added dropwise into a stirred solution of diethyl ether (50 mL). The resulting orange precipitate was collected by filtration, washed with 3 × 10 mL of diethyl ether, and dried *in vacuo*. Purification was performed by column chromatography using basic alumina as the support and MeCN as the eluent, and the product was collected as the second fraction. Yield: 45.2 mg (81.1%). $^{31}P\{^1H\}$ NMR (202.5 MHz, MeCN-d_3): δ 25.11 (s), −16.37 (s) ppm. FT-IR (KBr): ν_{CO} 2020 (vs), 1911 (vs), 1880 (vs) cm^{-1}. Anal. Calcd for $C_{74}H_{56}F_{12}N_4O_3P_6ClReRu$: C, 49.77; H, 3.16; N, 3.13. Found: C, 49.73; H, 3.34; N, 3.16.

$[(bpy)_2Os(C_3P_4)Re(CO)_3Cl](PF_6)_2$ (OsC_3P_4Re). $Re(CO)_5Cl$ (26.0 mg, 0.071 mmol) was refluxed with **OsC_3P_4** (52.0 mg, 0.033 mmol) in a MeCN (20 mL) and THF (5 mL) mixture for 24 h. The reaction mixture was then cooled to room temperature before the solvent was removed by a rotary evaporator. After the resulting brownish-green material was dissolved in ∼2 mL of MeCN, it was added dropwise into a 50 mL stirred solution of diethyl ether. The resulting green precipitate was collected by filtration, rinsed with 3 × 15 mL of diethyl ether, and dried *in vacuo*. Purification was performed by column chromatography using basic alumina as the support and MeCN as the eluent, and the product was collected as the second fraction. Yield:

(12) (a) Schmidbaur, H.; Pollok, T. *Angew. Chem., Int. Ed. Engl.* **1986**, *25*, 348−349. (b) Schmidbaur, H.; Manhart, S.; Schier, A. *Chem. Ber.* **1993**, *126*, 6, 2 389−2391. (c) Colquhoun, I. J.; McFarlane, W. *J. Chem. Soc., Dalton Trans.* **1982**, 1915−1920.

(13) (a) Buckingham, D. A.; Dwyer, F. P.; Goodwin, H. A.; Sargeson, A. M. *Aust. J. Chem.* **1964**, *17*, 325. (b) Kober, E. M.; Casper, J. V.; Sullivan, B. P.; Meyer, T. J. *Inorg. Chem.* **1988**, *27*, 4587.

(14) (a) Caspar, J. V.; Meyer, T. J. *J. Am. Chem. Soc.* **1983**, *105*, 5583−5590. (b) Caspar, J. V.; Sullivan, B. P.; Meyer, T. J. *Inorg. Chem.* **1984**, *23*, 2104−2109.

54.0 mg (87.1%). $^{31}P\{^1H\}$ NMR (202.5 MHz, MeCN-d_3): δ 96.57 (s), −24.11 (s) ppm. FT-IR (KBr): ν_{CO} 2032 (vs), 1941 (vs), 1908 (vs) cm^{-1}. Anal. Calcd for $C_{74}H_{56}F_{12}N_4O_3P_6ClOsRe$: C, 47.40; H, 3.01; N, 2.98. Found: C, 47.34; H, 3.27; N, 3.01.

$Cl(CO)_3Re(C_4P_4)$ (ReC_4P_4). To a refluxing solution of $\mathbf{C_4P_4}$ (261.7 mg, 0.332 mmol) in THF (40 mL) was added $Re(CO)_5Cl$ (57.0 mg, 0.157 mmol) in THF (20 mL) dropwise. After refluxing for 24 h, the reaction mixture was cooled to room temperature. The volume of the solution was reduced down to ~2 mL before being added dropwise into a stirred solution of hexanes (75 mL). The resulting orange precipitate was collected by filtration, washed with 3 × 15 mL of hexanes, and dried *in vacuo*. Purification was performed by column chromatography using basic alumina as the support and $CHCl_3$ as the eluent, and the product was collected as the first fraction. Yield: 82.5 mg (64.2%). $^{31}P\{^1H\}$ NMR (202.5 MHz, acetone-d_6): δ 21.40 (s), −8.92 (s) ppm. FT-IR (KBr): ν_{CO} 2026 (vs), 1948 (vs), 1907 (vs) cm^{-1}. Anal. Calcd for $C_{55}H_{40}O_3P_4ClRe$: C, 60.35; H, 3.68. Found: C, 60.57; H, 3.64.

$Cl(CO)_3Re(C_4P_4)Re(CO)_3Cl$ (ReC_4P_4Re). A solution containing $\mathbf{C_4P_4}$ (100.5 mg, 0.127 mmol) and $Re(CO)_5Cl$ (100.0 mg, 0.277 mmol) in THF (40 mL) was refluxed for 24 h, and the reaction mixture was cooled to room temperature. The volume of the solution was reduced down to ~2 mL before being added dropwise into a stirred solution of hexanes (125 mL). The resulting red precipitate was collected by filtration, washed with 3 × 15 mL of hexanes, and dried *in vacuo*. Purification was performed by column chromatography using basic alumina as the support and $CHCl_3$ as the eluent, and the product was collected as the second fraction. Crystals were obtained by first dissolving the red powder in a minimum amount of THF and then adding an equivalent amount of benzene. The solution mixture was stored at room temperature in a vented container. As the THF evaporated, red plates formed. Yield: 139.4 mg (78.4%). $^{31}P\{^1H\}$ NMR (202.5 MHz, acetone-d_6): δ −2.53 (s) ppm. ^{13}C NMR (125.7 MHz, THF-d_8): δ 135.18 (m, C═*C*═C), 133.76 (m, phenyl C_i), 132.25 (d, J_{CP} = 7.6 Hz, ═*C*P_2), 129.93 (s, phenyl, C_p), 129.3 (m, phenyl C_m and C_o). FT-IR (KBr mull): ν_{CO} 2030 (vs), 1960 (vs), 1900 (vs) cm^{-1}. Anal. Calcd for $C_{58}H_{40}O_6P_4Cl_2Re_2$: C, 49.75; H, 2.87. Found: C, 49.83; H, 2.88.

$[(bpy)_2Ru(C_4P_4)Re(CO)_3Cl](PF_6)_2$ (RuC_4P_4Re). A solution containing both $Re(CO)_5Cl$ (14.0 mg, 0.039 mmol) and $\mathbf{RuC_4P_4}$ (31.0 mg, 0.021 mmol) in a MeCN (20 mL) and THF (20 mL) mixture was heated at reflux for 24 h. Upon completion, the solution was allowed to cool to room temperature, and the solvent removed with the use of a rotary evaporator. The resulting reddish-brown material was dissolved in ~2 mL of MeCN. The 2 mL sample was dropped into a stirred solution of diethyl ether (50 mL). The resulting reddish-orange precipitate was collected by filtration, washed with 3 × 10 mL diethyl ether, and dried *in vacuo*. Purification was performed by column chromatography using basic alumina as the support and MeCN as the eluent, and the product was collected as the second fraction. Yield: 29.2 mg (77.4%). $^{31}P\{^1H\}$ NMR (202.5 MHz, MeCN-d_3): δ 20.18 (s), 13.56 (s) ppm. FT-IR (KBr): ν_{CO} 2015 (vs), 1880 (vs) cm^{-1}. Anal. Calcd for $C_{75}H_{56}F_{12}N_4O_3P_6ClReRu$: C, 50.10; H, 3.13; N, 3.11. Found: C, 50.14; H, 3.23; N, 3.12.

$[(bpy)_2Os(C_4P_4)Re(CO)_3Cl](PF_6)_2$ (OsC_4P_4Re). A solution of both $Re(CO)_5Cl$ (18.5 mg, 0.051 mmol) and $\mathbf{OsC_4P_4}$ (40.5 mg, 0.025 mmol) in a MeCN (20 mL) and THF (20 mL) mixture was heated at reflux for 24 h. Upon completion, the solution was allowed to cool to room temperature, and the solvent removed with the use of a rotary evaporator. The resulting brown material was dissolved in ~2 mL of MeCN and then added dropwise into a stirred solution of diethyl ether (50 mL). The resulting brown precipitate was collected by filtration, washed with 3 × 10 mL of diethyl ether, and dried in vacuo. Purification was performed by column chromatography using basic alumina as the support and MeCN as the eluent, and the product was collected as the second fraction. Yield: 35.5 mg (73.5%). $^{31}P\{^1H\}$ NMR (202.5 MHz, MeCN-d_3): δ 81.14 (s), −7.54 (s) ppm. FT-IR (KBr): ν_{CO} 2021 (vs), 1890 (vs) cm^{-1}. Anal. Calcd for $C_{75}H_{56}F_{12}N_4O_3P_6ClOsRe$: C, 47.73; H, 2.99; N, 2.96. Found: C, 47.62; H, 3.01; N, 3.01.

X-ray Structure Determination for ReC_3P_4Re. A yellow crystal of $Cl(CO)_3Re(\mathbf{C_3P_4})Re(CO)_3Cl\cdot 2(C_6H_6)$ with the dimensions 0.17 × 0.20 × 0.37 mm was mounted on a glass fiber and transferred to a Bruker CCD platform diffractometer. The SMART[15] program package was used to determine the unit cell parameters and for data collection (30 s/frame scan time for a hemisphere of diffraction data). The raw frame data was processed using SAINT[16] and SADABS[17] to yield the reflection data file. Subsequent calculations were carried out using the SHELXTL[18] program. The diffraction symmetry was 2/*m* and the systematic absences were consistent with the monoclinic space groups *Cc* or *C*2/*c*. It was later determined that the centrosymmetric space group *C*2/*c* was correct.

The structure was solved by direct methods and refined on F^2 by full-matrix least-squares techniques. The analytical scattering factors[19] for neutral atoms were used throughout the analysis. Hydrogen atoms were located from a difference Fourier map and refined (*x*,*y*,*z*) and *U*(iso) or included using a riding model. The molecule was a dimer, which was located on a 2-fold rotation axis. Atom C(26) was located directly on the 2-fold and was assigned a site-occupancy factor of 0.5. There were two molecules of benzene solvent present per dimeric formula unit. The solvent molecule defined by atoms C(30)−C(32) was located about a 2-fold axis, while that defined by atoms C(33)−C(35) was located about an inversion center. At convergence, wR2 = 0.0441 and GOF = 1.107 for 475 variables refined against 7460 unique data (as a comparison for refinement on *F*, R1 = 0.0195 for those 6911 data with $I > 2.0\sigma(I)$).

X-ray Structure Determination for ReC_4P_4Re. A red crystal of $Cl(CO)_3Re(\mathbf{C_4P_4})Re(CO)_3Cl\cdot 4(C_4H_8O)$ with the dimensions 0.03 × 0.16 × 0.17 mm was mounted on a glass fiber and transferred to a Bruker CCD platform diffractometer. The SMART[15] program package was used to determine the unit-cell parameters and for data collection (30 s/frame scan time for a hemisphere of diffraction data). The raw frame data was processed using SAINT[16] and SADABS[17] to yield the reflection data file. Subsequent calculations were carried out using the SHELXTL[18] program. The diffraction symmetry was 2/*m*, and the systematic absences were consistent with the monoclinic space groups *Cc* or *C*2/*c*. It was later determined that the centrosymmetric space group *C*2/*c* was correct.

The structure was solved by direct methods and refined on F^2 by full-matrix least-squares techniques. The analytical scattering factors[19] for neutral atoms were used throughout the analysis. Hydrogen atoms were included using a riding model. The molecule was a dimer, which was located about an inversion center. There were four molecules of THF solvent present per dimeric formula unit. The solvent molecules were disordered and were included with two components for each atom which were assigned site-occupancy factors of 0.5. The SAME[18] command was used to fix the geometry of the rings relative to that defined by O(5)−C(37). At convergence, wR2 = 0.0918 and GOF = 1.073 for 405 variables refined against 8421 unique data (as a comparison for refinement on *F*, R1 = 0.0454 for those 6507 data with $I > 2.0\sigma(I)$).

Results and Discussion

Synthetic Aspects. For the mono- and homobimetallic reactions with Re^I, the metal-to-ligand ratios can be altered in order to favor the production of the desired adduct. The addition of the metal starting material to a heated solution of the ligand, with the metal-to-ligand ratio 1:(1.7−2.2), favors the production of the monometallic complex. By having an excess amount of spacer, the formation of the monometallic complex was dominating. Conversely, if the ligand was added to a heated

(15) *SMART Software Users Guide, Version 4.21*; Bruker Analytical X-ray Systems, Inc.: Madison, WI, 1997.
(16) *SAINT Software Users Guide, Version 4.05*; Bruker Analytical X-ray Systems, Inc.: Madison, WI, 1997.
(17) Sheldrick, G. M. *SADABS*; Bruker Analytical X-ray Systems, Inc.: Madison, WI, 1997.
(18) Sheldrick, G. M. *SHELXTL Version 5.10*; Bruker Analytical X-ray Systems, Inc.: Madison, WI, 1997.
(19) *International Tables for X-ray Crystallography*, *Vol. C*; Kluwer Academic Publishers: Dordrecht, 1992.

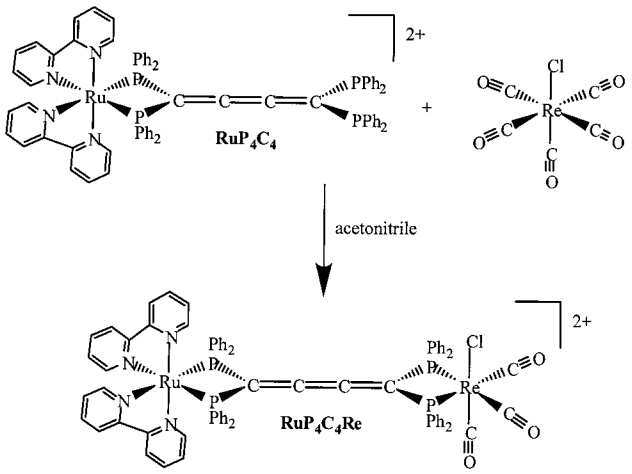

Figure 1. Representative synthesis of a heterobimetallic complex.

solution of the metal precursor with the metal-to-ligand ratio (2−2.2):1, the homobimetallic species was the major product isolated.

To synthesize the heterometallic complexes **RuC$_3$P$_4$Re** and **RuC$_4$P$_4$Re** (Figure 1), the ligand was first attached to the Ru^{II} center, which subsequently reacted with Re(CO)$_5$Cl in refluxing acetonitrile (82° C) for 24 h with a Ru:Re ratio of 1:1.5. The corresponding heterobimetallic complexes **OsC$_3$P$_4$Re** and **OsC$_4$P$_4$Re** were obtained under the same conditions but with a slightly more excess of Re(CO)$_5$Cl (Os:Re ratio of 2:1). More of the Re^{I} starting material was needed in the reaction of the Os^{II} complexes because the Os^{II} adducts were less reactive than the Ru^{II} ones. The presence of an excess of Re^{I} favored the reaction in the forward direction to give **OsC$_n$P$_4$Re** (n = 3, 4).

Upon completion of reactions and the removal of the THF portion of the solvent mixture, the remaining concentrated product/solvent mixture was added dropwise into a saturated aqueous solution of KPF_6 to obtain the solid products. There are two reasons to use the KPF_6/H_2O solution. First, the metal complexes with either +2 to +4 charges were slightly soluble in water. Saturating the water with KPF_6 salt increased the polarity of the solution to the point that the organic portion of the multicomponent complexes controlled the solubility of the overall complex and precipitated out of aqueous solution. The second reason was to ensure that the product was isolated as the PF_6 salt rather than a chloride salt. While the complexes with the PF_6^- counteranions are luminescent, the corresponding adducts with Cl^- counteranions are not.

Chromatographic methods were required in order to purify the desired products. In the isolation of the monometallic complexes, the major side products to be separated were the homobimetallic complexes and the monosubstituted complex, where a chloride was still coordinated to the Ru^{II} or Os^{II} center. The chromatographic separation in this system was possible partly due to the different cationic charges on these organometallic complexes. For the system containing only the Re^{I} centers, chloroform was used in the chromatographic separation. However, for the heterobimetallic Re^{I}/Ru^{II} and Re^{I}/Os^{II} complexes, acetonitrile was a better solvent for the chromatographic separation. This was due to the solubility characteristics imparted by the Os^{II} and Ru^{II} moieties connected via the cumulenic spacer to the Re^{I} moiety.

FAB/MS Analysis. A summary of the FAB/MS data is in Table 1. There are several apparent trends of the features in the data. The molecular ions were detected for the neutral monometallic complexes (**ReC$_2$P$_2$e**, **ReC$_3$P$_4$**, and **ReC$_4$P$_4$**) as well as the neutral homobimetallic ones (**ReC$_3$P$_4$Re** and **ReC$_4$P$_4$Re**). For the cationic heterobimetallic complexes containing either Ru^{II} or Os^{II}, the overall structures were found to be less robust than the complexes containing solely the Re^{I} center. The loss of the counterion PF_6^- occurred readily, as did the loss of F^- atoms. Even though the core structures were stable, loss of PPh_2

Table 1. Fast Atom Bombardment Mass Spectral (FAB/MS) Data

compound	MW (m/z), [rel int, %]	fragment assignment
ReC$_2$P$_2$e	702 [15]	M^+
	674 [30]	$M^+ - CO$
	667 [100]	$M^+ - Cl$
	646 [30]	$M^+ - 2CO$
	638 [15]	$M^+ - CO - Cl$
	618 [60]	$M^+ - 3CO$
	582 [10]	$M^+ - 3CO - Cl$
ReC$_3$P$_4$	1082 [55]	M^+
	1054 [20]	$M^+ - CO$
	1046 [15]	$M^+ - Cl$
	1026 [15]	$M^+ - 2CO$
	1018 [15]	$M^+ - CO - Cl$
	998 [5]	$M^+ - 3CO$
	915 [40]	$M^+ - PPh_2 + O$
	898 [10]	$M^+ - PPh_2$
	879 [90]	$M^+ - PPh_2 - Cl + O$
	863 [20]	$M^+ - PPh_2 - Cl$
	857 [100]	$M^+ - PPh_2 - 2CO + O$
	841 [100]	$M^+ - PPh_2 - 2CO$
	832 [100]	$M^+ - PPh_2 - 2CO + O$
	832 [35]	$M^+ - PPh_2 - CO - Cl$
	806 [15]	$M^+ - PPh_2 - 2CO - Cl$
ReC$_4$P$_4$	1095 [60]	M^+
	1067 [35]	$M^+ - CO$
	1059 [100]	$M^+ - Cl$
	1038 [80]	$M^+ - 2CO$
	1031 [30]	$M^+ - CO - Cl$
	1010 [55]	$M^+ - 3CO$
	1003 [30]	$M^+ - 2CO - Cl$
	910 [10]	$M^+ - PPh_2$
	845 [45]	$M^+ - PPh_2 - CO - Cl$
	825 [95]	$M^+ - PPh_2 - 3CO$
ReC$_3$P$_4$Re	1388 [30]	M^+
	1360 [20]	$M^+ - CO$
	1053 [100]	$M^+ - Cl$
	1332 [25]	$M^+ - 2CO$
	1297 [10]	$M^+ - 2CO - Cl$
ReC$_4$P$_4$Re	1400 [85]	M^+
	1072 [10]	$M^+ - CO$
	1365 [15]	$M^+ - Cl$
	1316 [10]	$M^+ - 2CO - Cl$
	1281 [15]	$M^+ - 3CO - Cl$
	1217 [45]	$M^+ - 4CO - 2Cl$
	1181 [45]	$M^+ - PPh_2 - Cl$
	1125 [95]	$M^+ - PPh_2 - 2CO - Cl$
	1095 [45]	$M^+ - PPh_2 - 3CO - Cl$
RuC$_3$P$_4$Re	1668 [45]	$M^+ - 3CO - Cl$
	1476 [100]	$M^+ - Re(CO)_3Cl$
	1331 [60]	$M^+ - Re(CO)_3Cl - PF_6$
	1186 [50]	$M^+ - Re(CO)_3Cl - 2PF_6$
RuC$_4$P$_4$Re	1472 [30]	$M^+ - 2PF_6$
	1440 [100]	$M^+ - 2PF_6 - Cl - CO$
	1287 [60]	$M^+ - 2PF_6 - PPh_2 - Cl$
	1267 [45]	$M^+ - 2PF_6 - PPh_2 - 2CO$
	1259 [60]	$M^+ - 2PF_6 - PPh_2 - Cl - CO$
	1231 [30]	$M^+ - 2PF_6 - PPh_2 - Cl - 2CO$
	1090 [45]	$M^+ - 2PF_6 - 2PPh_2 - Cl - CO + O$
OsC$_3$P$_4$Re	1748 [100]	$M^+ - PF_6 + O$
	1606 [60]	$M^+ - 2PF_6 + O$
	1586 [15]	$M^+ - 2PF_6$
	1566 [100]	$M^+ - 2PF_6 - Cl + O$
OsC$_4$P$_4$Re	1568 [10]	$M^+ - 2PF_6 - CO$
	1543 [15]	$M^+ - 2PF_6 - 2CO$
	1536 [40]	$M^+ - 2PF_6 - CO - Cl$
	1509 [25]	$M^+ - 2PF_6 - 2CO - Cl$
	1491 [100]	$M^+ - 2PF_6 - 3CO - Cl + O$
	1475 [95]	$M^+ - 2PF_6 - 3CO - Cl$

Table 2. Crystal Data and Structure Refinement for **ReC$_3$P$_4$Re** and **ReC$_4$P$_4$Re**

	ReC$_3$P$_4$Re	**ReC$_4$P$_4$Re**
empirical formula	$C_{57}H_{40}Cl_2O_6P_4Re_2$·2-($C_6H_6$)	$C_{58}H_{40}Cl_2O_6P_4Re_2$·4-($C_4H_8O$)
fw	1544.29	1688.50
cryst syst	monoclinic	monoclinic
space group	*C*2/*c*	*C*2/*c*
wavelength (Å)	0.71073	0.71073
temp (K)	158	158
a (Å)	18.0275(9)	25.3118(12)
b (Å)	18.9805(9)	15.1708(7)
c (Å)	19.3010(9)	19.7377(9)
α (deg)	90	90
β (deg)	110.5770(10)	109.9210(10)
γ (deg)	90	90
volume (Å^3)	6182.9(5)	7125.8(6)
Z	4	4
F(000)	3032	3360
ρ_{calc} (mg m^{-3})	1.659	1.574
μ (mm^{-1})	4.154	3.616
cryst size (mm^3)	0.37 × 0.20 × 0.17	0.17 × 0.16 × 0.03
no. of reflns collected	19960	22278
no. of unique reflns	7460	8421
$S(F^2)$[a]	1.107	1.073
final *R* indices[b] [$I > 2\sigma(I)$]	R1 = 0.0195 wR2 = 0.0428	R1 = 0.0454 wR2 = 0.0828
R indices (all data)[b]	R1 = 0.0227 wR2 = 0.0441	R1 = 0.0711 wR2 = 0.0918

[a] S = goodness of fit = $[\sum[w(F_o^2 - F_o^2)^2]/(n-p)]^{1/2}$, where n is the number of reflections and p is the total number of parameters refined. [b] $R1 = \sum||F_o| - |F_c||/\sum|F_o|$ and $wR2 = [\sum[w(F_o^2 - F_o^2)^2]/\sum[w(F_o^2)^2]]^{1/2}$, $w = 1/\sigma^2(|F_o|)$.

groups was observed, coinciding with the results observed for the complexes with only the Ru^{II} or Os^{II} centers.[3] The loss of CO and Cl units from the Re^I core was also detected. The addition of one, two, or three oxygen atoms was found in fragments, even though all of the complexes were shown to be air stable from both $^{31}P\{^1H\}$ NMR and crystallographic data. Such additions of oxygen atoms were observed to be characteristic for systems with polyphosphine spacers.[3,6]

Crystal Structure Determination. The structures of **ReC$_3$P$_4$Re** and **ReC$_4$P$_4$Re** were obtained by single-crystal X-ray structure determination. A summary of the crystallographic data appears in Table 2. Selected bond lengths and bond angles are listed in Table 3. The ORTEP plot of **ReC$_3$P$_4$Re** is shown in Figure 2 (excluding the two benzene molecules, which crystallize as part of the unit cell). The refinements converged to R1 = 1.95% and wR2 = 4.24% with $I > 2\sigma(I)$ and R1 = 2.27%, wR2 = 4.41%, and S = 1.107 for 7460 unique reflections, 475 variables, and 60 restraints. The molecular unit consists of two Re(CO)$_3$Cl units bridged by the **C$_3$P$_4$** spacer. The metal-to-metal distance was 8.721 Å, with a dihedral angle (θ) of 91.9° defined by the two planes resulting from P(1)−Re(1)−P(2) and P(1′)−Re(1′)−P(2′). For an odd-numbered cumulenic chain, θ was expected to be 90.0°. The observed distortion is presumably due to steric interactions among the bulky phenyl groups. The C(25)−C(26)−C(25′) bond angle of the cumulenic carbon chain was found to be roughly linear (176.9°). The central C(26) was found to lie directly on the 2-fold axis of the molecule; therefore both C═C bond lengths were equivalent. Each Re^I moiety was octahedral with three carbonyl ligands in a facial arrangement.

The ORTEP plot of **ReC$_4$P$_4$Re** is shown in Figure 3 (excluding the four THF molecules, which crystallize as part of the unit cell). The refinements converged to R1 = 4.54% and wR2 = 8.28% with $I > 2\sigma(I)$ and R1 = 7.11%, wR2 = 9.18%, and S = 1.073 for 8421 unique reflections, 405 variables, and 60 restraints. The molecular unit consists of two Re(CO)$_3$Cl units bridged by the **C$_4$P$_4$** spacer. The metal-to-metal distance was 10.050 Å, which is 1.33 Å longer than the Re^I−Re^I distance in **ReC$_3$P$_4$Re**. The dihedral angle for **ReC$_4$P$_4$Re**, defined by the two planes containing P(1)−C(25)−P(2) and P(1′)-C(25′)−P(2′), was found to be 0.0°, which is expected for an even-numbered cumulenic chain. Because of a longer carbon chain length, the phenyl groups are no longer close enough to each other as to cause the distortion away from the coplanar arrangement. The bond angles for C(25)−C(26)−C(26′) and C(26)−C(26′)−C(25′) of the cumulenic carbon chain were found to be more linear (178.8°) than for the C$_3$ carbon chain in **ReC$_3$P$_4$Re** (176.9°), presumably due to the decrease in steric interactions among the phenyl groups. The 2-fold axis of the molecule was found to pass the center of the double bond between C(26) and C(26′). The C═C bond lengths of the cumulenic group contain the characteristic "long−short−long" pattern found for other butatrienes.[12b] As in **ReC$_3$P$_4$Re**, each Re^I moiety in **ReC$_4$P$_4$Re** is octahedral, with the three carbonyl ligands in a facial arrangement with the chloride perpendicular to the P(1)−Re(1)−P(2) plane.

For both crystal structures the bite angles, defined by the atoms P(1)−Re(1)−P(2), were found to be 70.33° and 70.43° for the C$_3$ and C$_4$ adducts, respectively. These values are consistent with but slightly smaller than the average bite angle (71.53°) found for diphenylphosphinomethane (dppm) coordinated to different transition metal centers.[20] Although the angles about a sp^2-hybridized carbon atom should theoretically be 120°, the angle of ∠P(1)−C(25)−P(2) for **ReC$_3$P$_4$Re** and **ReC$_4$P$_4$Re** was found to be 100.73° and 101.92°, respectively. These observed decreases in the angles are presumably caused by the four-membered ring structure at the Re^I center.

IR Analysis. The IR carbonyl stretches for compounds containing the Re(CO)$_3$Cl units are listed in Table 4. Except for **RuC$_4$P$_4$Re** and **OsC$_4$P$_4$Re**, every compound possessed three very strong signals in the carbonyl region between 2032 and 1880 cm^{-1} (Figure 4a). These data represent an apparent shift to lower energies with respect to the starting material Re(CO)$_5$Cl that appear between 2155 and 1854 cm^{-1}.[21] The similarity in the IR spectra of these compounds suggests that they all have the same core structure around the Re^I center. From the aforementioned crystal structures for **ReC$_3$P$_4$Re** and **ReC$_4$P$_4$Re**, it was observed that each Re^I center independently possessed C_s symmetry with the carbonyl ligands in a facial arrangement, one carbonyl *trans* to the chlorine atom and the other two carbonyls *trans* to the chelating diphenylphosphino groups (Figure 5a). Three IR-active carbonyl modes are expected for the Re^I centers which contain the local C_s symmetry (2A′ + A″).[22,23] The highest energy peak between 2032 and 2015 cm^{-1} has been assigned as the ν(CO) for the CO that is *trans* to the chlorine atom. Since the chlorine ligand is less electron donating than the diphenylphosphino groups, less back-bonding will occur from the Re^I metal to the *trans*$_{Cl}$ CO antibonding orbital. This effect will give rise to a higher bond order in the CO unit, shifting the ν(CO) to a higher energy relative to the two ν(CO) bands (between 1960 and 1880 cm^{-1}) from the CO groups that are *trans* to the diphenylphosphino units.[24,25]

Compounds **RuC$_4$P$_4$Re** and **OsC$_4$P$_4$Re** exhibit only two CO stretches; the higher energy peak is also assigned (as above) to the *trans*$_{Cl}$ CO, while the lower energy peak appears to be a

(20) Dierkes, P.; van Leeuwen, P. *J. Chem. Soc., Dalton Trans.* **1999**, 1519−1529.
(21) Kaesz, H. D.; Bau, R.; Hendrickson, D.; Smith, J. M. *J. Am. Chem. Soc.* **1967**, *89*, 2844−2851.
(22) Benkstein, K. D.; Hupp, J. T.; Stern, C. L. *Inorg. Chem.* **1998**, *37*, 5404−5405.
(23) Abel, E. W.; Tyfield, S. P. *Can. J. Chem.* **1969**, *47*, 4627−4633.

Table 3. Selected Bond Distances (Å) and Bond Angles (deg) for Complexes **ReC$_3$P$_4$Re** and **ReC$_4$P$_4$Re**

bond	**ReC$_3$P$_4$Re**	**ReC$_4$P$_4$Re**	angle	**ReC$_3$P$_4$Re**	**ReC$_4$P$_4$Re**
Re(1)−C(27)	1.918(2)	2.009(6)	C(27)−Re(1)−Cl(1)	179.30(7)	179.07(15)
Re(1)−C(28)	1.966(2)	1.954(6)	C(28)−Re(1)−P(2)	167.62(7)	167.50(17)
Re(1)−C(29)	1.950(2)	1.950(6)	C(29)−Re(1)−P(1)	168.77(7)	167.52(17)
Re(1)−P(1)	2.4789(5)	2.4616(13)	P(1)−Re(1)−P(2)	70.33(17)	70.43(4)
Re(1)−P(2)	2.4654(5)	2.4641(13)	P(1)−C(25)−P(2)	100.73(9)	101.9(2)
Re(1)−Cl(1)	2.4869(6)	2.4673(14)	C(25)−C(26)−C(25′)	176.9(3)	
O(1)−C(27)	1.139(3)	1.017(6)	C(25)−C(26)−C(26′)		178.8(7)
O(2)−C(28)	1.137(3)	1.144(6)			
O(3)−C(29)	1.142(3)	1.145(7)			
P(1)−C(25)	1.842(2)	1.832(5)			
P(2)−C(25)	1.855(2)	1.826(5)			
C(25)−C(26)	1.303(2)	1.324(6)			
C(26)−C(26)′		1.260(9)			

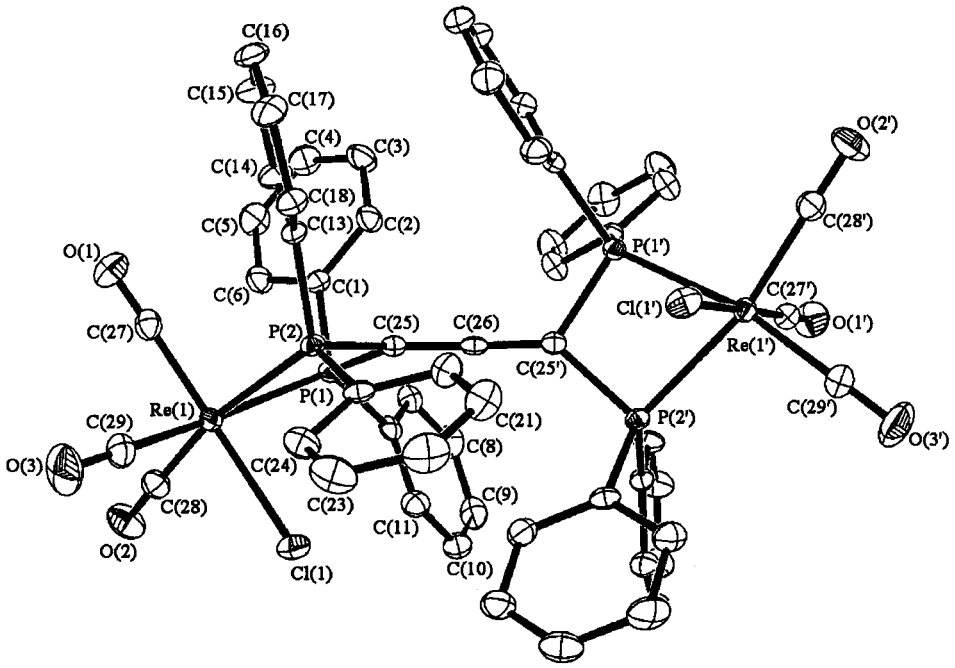

Figure 2. ORTEP plot of **ReC$_3$P$_4$Re** with thermal ellipsoids plotted at 50% probability. For clarity hydrogen atoms have been omitted.

broaden combination of the two *trans*$_P$ CO (Figure 4b). This effect can be explained by the increased electronic communication associated with the **C$_4$P$_4$** spacer.[3] An increase in electron delocalization from the diphenylphosphino chelates in the polyphosphine spacer will cause a sufficient perturbation on the ν(CO) vibrational modes, rendering them indistinguishable. Previously for systems that contained three CO in a facial arrangement with chelating N-donating ligands, only one band was observed for the two CO *trans* to the chelating N-ligands.[26,27] Another possible interpretation of the observation of only two ν(CO) bands for the complexes **RuC$_4$P$_4$Re** and **OsC$_4$P$_4$Re** could be that the carbonyl groups are not in a facial arrangement but rather a meridial arrangement.[23] This arrangement would place two of the carbonyl groups *trans* with respect to each other, rendering their ν(CO) stretches equivalent, while the third CO would be *trans* to one of the diphenylphosphino groups in the spacer (Figure 5b). Since the phosphine would be a better electron donor than the π-acidic carbonyl ligands, it would be expected, however, that the *trans*$_P$ ν(CO) would be shifted to a lower energy than the broad ν(CO) band that corresponds to the CO groups *trans* to each other. This is a contradiction to the observed IR spectra that exhibit the broad signal to be of lower energy. Hence, the actual observation is consistent with the facial arrangement argument. In addition, the facial arrangement would also be the more thermodynamically stable one of the two possible configurations.[23]

As mentioned earlier, there was very little change of the three ν(CO) bands in most of the Re^I complexes. The three Re^I monometallic complexes exhibited very similar ν(CO) frequencies, with 2026, 1944, and 1911 cm^{-1} for **ReC$_3$P$_4$**, 2026, 1948, and 1907 cm^{-1} for **ReC$_4$P$_4$**, as well as 2029, 1952, and 1895 cm^{-1} for **ReC$_2$P$_2$e**. Likewise, the Re^I homobimetallic complexes had ν(CO) similar to their corresponding monometallic adducts: 2026, 1946, and 1914 cm^{-1} for **ReC$_3$P$_4$Re**, and 2030, 1960, and 1900 cm^{-1} for **ReC$_4$P$_4$Re**. In the Os^{II}-containing heterobimetallic complexes, there was a minor shift to lower energy for the *trans*$_P$ ν(CO). For the Ru^{II}-containing heterobimetallic species **RuC$_n$P$_4$Re** (n = 3, 4), a shift to even lower energy was observed in the *trans*$_P$ ν(CO). For **RuC$_3$P$_4$Re**, the shift was about 35 cm^{-1}. For **RuC$_4$P$_4$Re**, the combined *trans*$_P$ ν(CO) occurred at 1880 cm^{-1}, about 80 cm^{-1} shift toward lower energy when compared with *trans*$_P$ ν(CO) in **ReC$_4$P$_4$Re**. The shift from the lower energy peak of the *trans*$_P$ ν(CO) in

(24) Huhmann-Vincent, J.; Scott, B. L.; Kubas, G. J. *Inorg. Chem.* **1999**, *38*, 115−124.
(25) Edwards, D. A.; Marshalsea, J. *J. Organomet. Chem.* **1977**, *131*, 73−90.
(26) Pfennig, B. W.; Cohen, J. L.; Sosnowski, I.; Novotny, N. M.; Ho, D. M. *Inorg. Chem.* **1999**, *38*, 606−612.
(27) Schoonover, J. R.; Strouse, G. F.; Dyer, R. B.; Bates, W. D.; Chen, P. Y.; Meyer, T. J. *Inorg. Chem.* **1996**, *35*, 273−274.

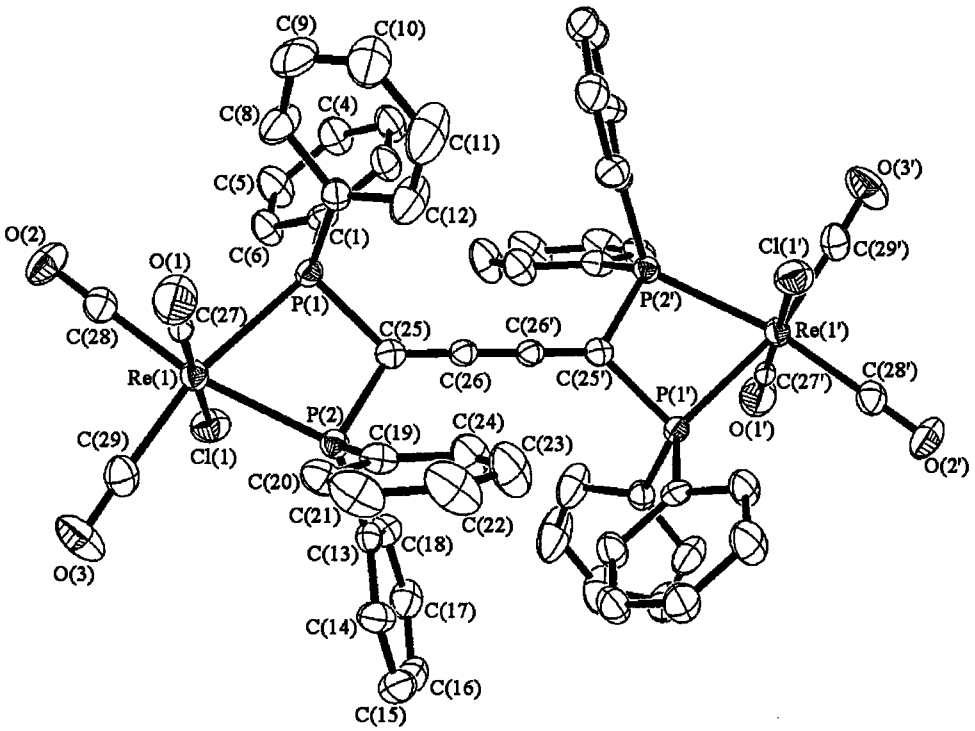

Figure 3. ORTEP plot of **ReC$_4$P$_4$Re** with thermal ellipsoids plotted at 50% probability level. For clarity hydrogen atoms have been omitted.

Table 4. IR[a] Spectroscopic Data of the Carbonyl Signals[b] for Re^{I} Complexes

compound	ν_{CO} trans$_{Cl}$ (cm^{-1})	ν_{CO} trans$_{P}$ (cm^{-1})	
ReC$_3$P$_4$	2026	1944	1911
ReC$_4$P$_4$	2026	1948	1907
ReC$_2$P$_2$e	2029	1952	1895
ReC$_3$P$_4$Re	2026	1946	1914
ReC$_4$P$_4$Re	2030	1960	1900
RuC$_3$P$_4$Re	2020	1911	1880
RuC$_4$P$_4$Re	2015	1880	
OsC$_3$P$_4$Re	2032	1941	1908
OsC$_4$P$_4$Re	2021	1890	

[a] Measured as KBr pellets. [b]Every signal measured was very strong (vs).

ReC$_n$P$_4$Re (n = 3, 4) to the combined trans$_P$ ν(CO) in **RuC$_4$P$_4$Re** was 20 cm^{-1}. These shifts are due to an increase of electron donation from the Ru^{II} center through the spacer to the Re^{I} center and subsequently into the antibonding orbital of the CO ligand. A greater shift (of the carbonyl stretches) to lower energies occurred for **RuC$_4$P$_4$Re** and **OsC$_4$P$_4$Re**, along with the observation of the overlapping ν(CO) signals. These are indicative of a greater electronic communication through the **C$_4$P$_4$** with respect to complexes of **C$_3$P$_4$**.

^{31}P{^{1}H} NMR Analysis. Analysis of the new complexes by ^{31}P{^{1}H} NMR has proven to provide substantial information as to the identification and the purity of samples.[6,28−30] The ^{31}P-{^{1}H} NMR data for all new Re^{I} complexes are listed in Table 5. Singlets were observed for both the noncoordinated diphenylphosphino groups and the coordinated M−PPh$_2$ units, except in **ReC$_3$P$_4$Re**. Regarding the two observed doublets in the ^{31}P NMR spectrum of **ReC$_3$P$_4$Re**, the aforementioned X-ray structural determination revealed a structural distortion possibly due to the steric interaction between the bulky phenyl groups. Such steric distortion may cause the two *cis*-PPh$_2$ units on the same Re^{I} centers to be unequivalent and results in two ^{31}P NMR signals with a small *cis*-coupling J_{P-P} constant of *ca.* 36 Hz. Furthermore, the maximum symmetry the molecule may have in solution is C_2, which may also result in the pairwise

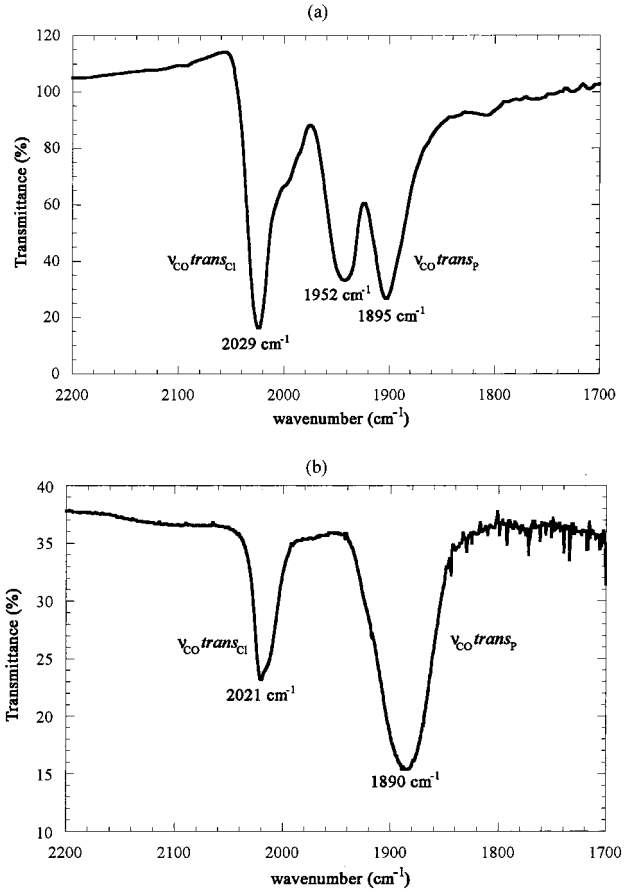

Figure 4. (a) Representative carbonyl region of the IR spectrum for **ReC$_2$P$_2$e** depicting three very strong signals. (b) Region of the IR spectrum for **OsC$_4$P$_4$Re** depicting only two very strong signals.

inequivalence of the four P atoms. As a comparison, the steric interaction within the corresponding homobimetallic species **ReC$_4$P$_4$Re** is decreased due to an increased carbon chain length in the bridging unit, and the single-crystal structure determi-

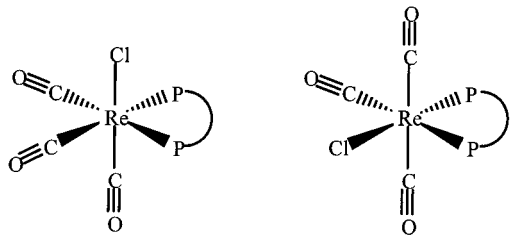

Figure 5. The two possible arrangements for the Re^{I} core.

nation confirmed an ideal coplanar arrangement, with a dihedral angle of 0.0°, of the two $Re(CO)_3Cl(P)_2$ units. As a result, only one singlet was observed in the ^{31}P NMR spectrum.

For the assignment of signals, the chemical shifts for the $Re^{I}-PPh_2$ units appeared between −1.43 and −12.75 ppm in **ReC$_2$P$_2$e**, **ReC$_3$P$_4$Re**, and **ReC$_4$P$_4$Re**, and at −8.92 and −13.30 ppm in **ReC$_3$P$_4$** and **ReC$_4$P$_4$**, respectively. The two other signals at 22.80 and 21.40 ppm are assigned to the free noncoordinated $-PPh_2$ units. For the monometallic complexes **ReC$_3$P$_4$**, **ReC$_4$P$_4$**, and **ReC$_2$P$_2$e** the signals for the noncoordinated phosphines in the $^{31}P\{^1H\}$ NMR spectra were shifted downfield, while the coordinated phosphine signals were shifted upfield with respect to the free ligands. This behavior is indicative of an inductive "pulling" of the electrons away from the noncoordinated $-PPh_2$ units. Presumably, this effect is caused by the CO units on the Re^{I} center withdrawing electron density across the spacer. Therefore, the $-PPh_2$ units coordinated to the Re^{I} center experienced an increase in shielding from the electrons inductively withdrawn from the noncoordinated $-PPh_2$ units.

Similarly, the ^{31}P NMR signals for the heterobimetallic complexes can also be assigned. The signals at negative ppm chemical shifts represented the $Re^{I}-PPh_2$ units, while the signals at positive chemical shifts signify the $Ru^{II}-PPh_2$ and $Os^{II}-PPh_2$ units. While the Os^{II} resulted in signals significantly shifted to above +80 ppm, the $Ru^{II}-PPh_2$ appeared between +20 and +25 ppm. Even though **RuC$_4$P$_4$Re** had two signals at positive chemical shifts, the signal at 20.18 ppm was assigned to $Ru^{II}-PPh_2$ due to the proximity with the signal of **RuC$_4$P$_4$Re** at 25.11 ppm. As observed for the monometallic complexes, the carbonyl groups of the Re^{I} unit inductively shield the $Re^{I}-PPh_2$ units while deshielding the $Ru^{II}-PPh_2$ and $Os^{II}-PPh_2$ units.

It was shown previously[25,31] that in similar rhenium tricarbonyl systems the coordinated phosphorus signal of the chelating bisphosphine ligand (e.g., dppm) was shifted upfield with respect to the free ligand. This is in agreement with the above assignments for the $Re^{I}-PPh_2$ signals in this system. The electrons of the noncoordinating phosphines were inductively "pulled" through the cumulenic backbone toward the coordinated phosphines due to the back-bonding of the rhenium metal to the two *trans* carbonyls. Likewise, the phosphines coordinated to the Re^{I} center in the heterobimetallic complexes were also shifted upfield.

Redox Characteristics and Electronic Communication. Cyclic voltammetry (CV) has been a very important analytical tool for studying the electrochemical behavior of a variety of chemical systems in the past two to three decades.[32−34] It can be used to study the ground-state electronic communication of multicomponent supramolecular systems.[1h,4b,g,7e,35] By following the redox behavior of a given system, it then becomes possible to devise a way to control that behavior. For a system to be considered useful in the regime of molecular devices, that system must have electronic properties that are not only observable but also tunable.[1h,2,7c,35−37] By varying the redox potentials and consequently modulating the energetics of electron transport, the movement and storage of electrons within supramolecular systems can be possible. Several groups have been concerned with the redox behavior of one-dimensional rigid rodlike supramolecular systems. Our group have reported the modulation of redox potentials and the level of electronic communications between redox-active termini using Ru^{II} and Os^{II} complexes with polyphosphine/cumulene spacers.[3,6] Gladysz *et al.*[1f,h,11b] have reported the modification of redox communication between two metal units directly linked by acetylenic (polyyne) units with variable chain lengths. Lapinte and co-workers[7a,38] have also described the effect of different spacer lengths on the electrochemical behavior of the same metal-based unit in different oxidation states. It is anticipated that the rigidity and orientation of the spacers with organic linkage components can alter and manipulate the redox behavior of the metal termini.[3,39]

The results of electrochemical studies on the new compounds containing the mixed Re^{I}/Ru^{II} and Re^{I}/Os^{II} units are listed in Table 6. No reversible redox potential was observed for the Re^{I} metal center, but those attributed to the $Os^{II/III}$ and $Ru^{II/III}$ were observed to be pseudoreversible. Upon comparison of the heterobimetallic **MC$_n$P$_4$Re** (n = 3, 4, M = Ru, Os) with the corresponding Os^{II} and Ru^{II} monometallic species **MC$_n$P$_4$** (n = 3, 4, M = Ru, Os) previously reported,[3] similar characteristics were observed. For **RuC$_3$P$_4$Re** and **OsC$_3$P$_4$Re**, there were three redox waves corresponding to the metal oxidation at a positive potential, as well as the reduction of the **C$_3$P$_4$** spacer and the bipyridyl ligand at negative potentials. Alternatively, cyclic voltammograms for **RuC$_4$P$_4$Re** and **OsC$_4$P$_4$Re** displayed one metal-based oxidation and two bipyridine reductions, as observed before for the corresponding monometallic complexes with the same spacer. Interestingly, the longer C_4-spacer was not reduced within the CV scan range of this study, but the shorter **C$_3$P$_4$** was. A similar observation was also found in Ru^{II} and Os^{II} mono- and homobimetallic species with the same spacers.[3,6]

The longer **C$_4$P$_4$** spacer also caused the oxidation potentials of both Os^{II} and Ru^{II} to shift to lower values with respect to the corresponding complexes with **C$_3$P$_4$**. The $Ru^{II/III}$ redox couple of **RuC$_3$P$_4$Re** (+1.46 V) was shifted to a lower potential by 450 mV in **RuC$_4$P$_4$Re** (+1.01 V). Similarly, the $Os^{II/III}$ redox couple was shifted 520 mV to a less positive potential when

(28) Pregosin, P. S.; Kunz, R. W. *31P and 13C NMR of Transition Metal Phosphine Complexes*; Springer-Verlag: Berlin, 1979.
(29) Beringhelli, T.; Dalfonso, G.; Freni, M.; Minoja, A. P. *Inorg. Chem.* **1996**, *35*, 2393−2395.
(30) Benn, R. *Transition Metal Nuclear Magnetic Resonance*; Pregosin, P. S., Ed.; Amsterdam, Netherlands, 1991; Chapter 4.
(31) Carriedo, G. A.; Rodriguez, M. L.; Garciagranda, S.; Aguirre, A. *Inorg. Chim. Acta* **1990**, *178*, 101−106.
(32) Kissinger, P. T.; Heineman, W. R. *J. Chem. Educ.* **1983**, *60*, 702−706.
(33) Heinze, J. *Angew. Chem., Int. Ed. Engl.* **1984**, *23*, 831−918.
(34) Maloy, J. T. *J. Chem. Educ.* **1983**, *60*, 285−289.
(35) Patoux, C.; Launay, J. P.; Beley, M.; Chodorowski-Kimmes, S.; Collin, J. P.; James, S.; Sauvage, J. P. *J. Am. Chem. Soc.* **1998**, *120*, 3717−3725.
(36) Lehn, J. M. *Angew. Chem., Int. Ed. Engl.* **1990**, *29*, 1304−1319.
(37) Harriman, A.; Ziessel, R. *Coord. Chem. Rev.* **1998**, *171*, 331−339.
(38) Le Narvor, N.; Lapinte, C. *C. R. Acad. Sci. Ser. II C* **1998**, *1*, 745−749.
(39) Balzani, V.; Juris, A.; Venturi, M.; Campagna, S.; Serroni, S. *Chem. Rev.* **1996**, *96*, 759−833.

Table 5. $^{31}P\{^{1}H\}$ NMR Spectroscopic Data of Re^{I} Complexes[a]

complex	noncoord ^{31}P (ppm)	Re−P ^{31}P (ppm)	complex	Re−P ^{31}P (ppm)	Ru−P or Os−P ^{31}P (ppm)
ReP_4C_3	22.80 (s)	−13.30 (s)	**RuP_4C_3Re**	−16.37 (s)	25.11 (s)
ReP_4C_4	21.40 (s)	−8.92 (s)	**RuP_4C_4Re**	13.56 (s)	20.18 (s)
ReP_2C_2e		−8.41 (s)	**OsP_4C_3Re**	−24.11 (s)	96.57 (s)
ReP_4C_3Re		−12.75 (d, J_{P-P} = 35.7 Hz)	**OsP_4C_4Re**	−7.54 (s)	81.14 (s)
		−1.43 (d, J_{P-P} = 35.7 Hz)			
ReP_4C_4Re		−2.53 (s)			

[a] Only the chemical shifts associated with the core structure are presented here. A characteristic septet was observed for each complex corresponding to the PF_6^- counteranions centered between δ −144 and −145 ppm.

Table 6. Formal Potentials (vs SCE) for Ru^{II} and Os^{II} Complexes Containing Re^{I}

complex	$Ru^{II/III}$ $E_{1/2}$, V (ΔE_p, mV)	$Os^{II/III}$ $E_{1/2}$, V (ΔE_p, mV)	$P_4C_3^{0/-}$ $E_{1/2}$, V (ΔE_p, mV)	1st bpy$^{0/-}$ $E_{1/2}$, V (ΔE_p, mV)	2nd bpy$^{0/-}$ $E_{1/2}$, V (ΔE_p, mV)
RuP_4C_3Re	+1.46 (1e$^-$, 100)		−1.18 (1e$^-$, 70)	−1.42 (1e$^-$, 82)	
RuP_4C_4Re	+1.01 (1e$^-$, 146)			−1.40 (1e$^-$, 74)	−1.63 (1e$^-$, 65)
OsP_4C_3Re		+1.13 (1e$^-$, 104)	−1.12 (1e$^-$, 88)	−1.35 (1e$^-$, 74)	
OsP_4C_4Re		+0.61 (1e$^-$, 80)		−1.20 (1e$^-$, 84)	−1.42 (1e$^-$, 94)

comparing **OsC_3P_4Re** and **OsC_4P_4Re**. Presumably the longer **C_4P_4** had a greater number of delocalized π-electrons and was a better σ-donor than **C_3P_4**. When an increased amount of σ-donation was contributed to the metal center, there will be more electron density residing on the metal, thereby causing the redox couple to shift to a less positive value.[3a]

The metal-based oxidations for the heterobimetallic **MC_nP_4Re** (M = Ru^{II}, Os^{II}) complexes, though slightly different, were found to be consistent with the oxidation potentials of the previously reported monometallic complexes **MC_nP_4** (M = Ru^{II}, Os^{II}).[3,6] For **RuC_3P_4Re**, the $Ru^{II/III}$ oxidation occurred at +1.46 V, which was a 90 mV shift from that of the corresponding monometallic species **RuC_3P_4** (+1.55 V). For **RuC_4P_4Re**, the $Ru^{II/III}$ oxidation occurred at +1.01 V, only a 60 mV change from the corresponding **RuC_4P_4** monometallic species (+1.07 V). This similarity was also observed for the $Os^{II/III}$ redox couple in **OsC_3P_4Re** and the corresponding **OsC_3P_4**, where there was only a 10 mV difference in the oxidation potentials (+1.13 V and +1.12 mV, respectively). However, the complex **OsC_4P_4Re** (+0.61 V for $Os^{II/III}$) experienced a much larger shift in the oxidation potential (190 mV) with respect to the corresponding **OsC_4P_4** complex (+0.80 V). Such a low oxidation potential (+0.61 V) suggested that the Os^{II} center in **OsC_4P_4Re** was much easier to oxidize.

Electronic Absorption, Emission, and Lifetimes. The ground-state absorption maxima and extinction coefficients from the electronic absorption spectra of all new compounds are listed in Table 7. All of the complexes exhibit ligand-centered charge transfer (^{1}LC) features involving the bridging polyphosphine spacer in the visible region of 300−395 nm. The extinction coefficients ($\epsilon \sim 10^3-10^4$ M^{-1} cm^{-1}) are an order of magnitude more intense than those in a similar system containing non-polyene polyphosphine ligands ($\epsilon \approx 10^2-10^3$ M^{-1} cm^{-1}).[21] This observation may result from the extensive delocalization of electrons through the cumulenic framework. The mono- and homobimetallic complexes **ReC_4P_4** and **ReC_4P_4Re** have one more ^{1}LC charge transfer event than the corresponding **C_3P_4**-containing complexes in the region attributed to the polyphosphine spacer (Table 7). Presumably, the addition of another π-bond appears to facilitate the delocalization of electrons which may lower the π-antibonding orbitals, causing another charge transfer band to appear at lower energy. Once a Ru^{II} or Os^{II} polypyridyl group is attached to **C_4P_4**, the higher energy ^{1}LC band is no longer observable. Instead, they exhibit a second stronger type of ^{1}LC charge transfer involving the ancillary bpy ligands with well-known and typical extinction coefficients ($\epsilon \approx 10^4-10^5$ M^{-1} cm^{-1}).[22,23]

Table 7. Absorption Maxima from the Electronic Spectra of the Re^{I} Complexes

	λ_{abs}, nm (ϵ, M^{-1} cm^{-1})			
	ligand-centered CT		Re, Ru, or Os-based	
complex	N-bpy	P-spacer	^{1}MLCT	Os ^{3}MLCT
ReC_2P_2e		330 (9535)	420 (6070)	
ReC_3P_4		320 (11 889)	420 (4790)	
ReC_4P_4		300 (21 280)	465 (7990)	
		395 (8400)		
ReC_3P_4Re		350 (8120)	435 (sh, 530)	
ReC_4P_4Re		300 (14 520)	475 (2260)	
		370 (7640)		
RuC_3P_4Re	285 (30 580)	360 (6780)	450 (2155)	
RuC_4P_4Re	290 (35 635)	330 (14 400)	450 (3530)	
OsC_3P_4Re	290 (64 100)	345 (20 430)	440 (8100)	550 (sh, 1250)
OsC_4P_4Re	290 (100 950)	390 (17 240)	460 (15 540)	595 (3480)

The mono- and homobimetallic Re^{I} complexes also exhibit absorption maxima in the region 420−460 nm (Figure 6a) which have been previously assigned as a Re-based transition for a similar system.[40−42] Whereas in the earlier study the absorption bands were extremely weak (ϵ < 20 M^{-1} cm^{-1}), leading to an

(40) (a) Ramsis, M. N. *Monatsh. Chem.* **1993**, *124*, 849−855. (b) Wrighton, M. S.; Morse, D. L.; Gray, H. B.; Ottensen, K. K. *J. Am. Chem. Soc.* **1976**, *98*, 1111. (c) Giordano, P. J.; Wrighton, M. S. *J. Am. Chem. Soc.* **1979**, *101*, 2888.
(41) Dahlgren, R. M.; Zink, J. I. *Inorg. Chem.* **1977**, *16*, 3154.
(42) (a) Lees, A. J. *Comments Inorg. Chem.* **1995**, *17*, 319−346. (b) Kern, J.-M.; Sauvage, J.-P.; Weidmann, J.-L.; Armaroli, N.; Flamigni, L.; Ceroni, P.; Balzani, V. *Inorg. Chem.* **1997**, *36*, 5329−5338.

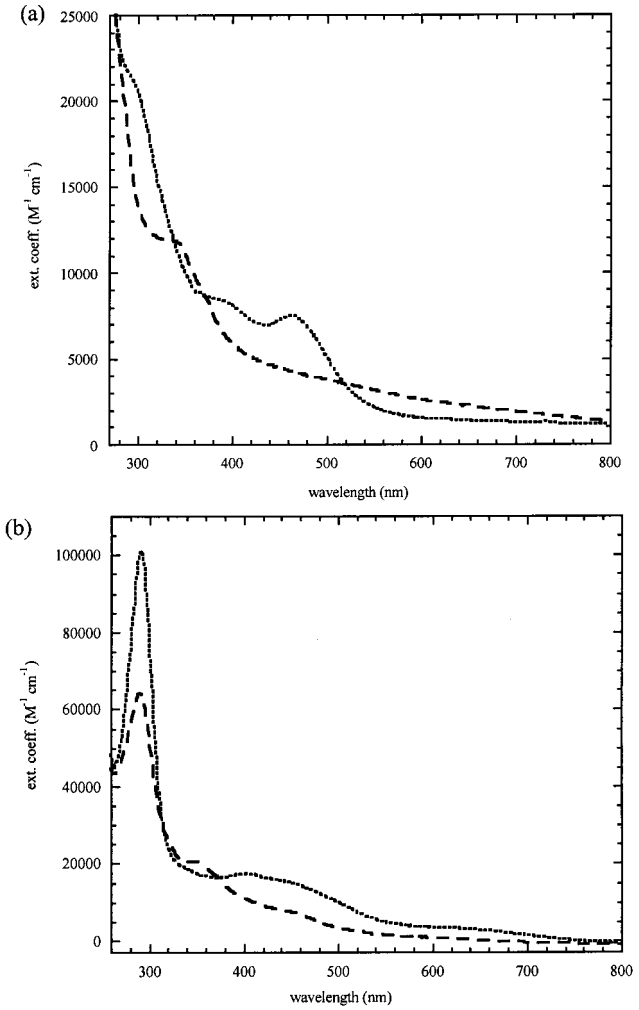

Figure 6. (a) Comparison of the electronic absorption spectra between (a) $\mathbf{ReC_3P_4}$ (- - -) and $\mathbf{ReC_3P_4}$ (···) and (b) $\mathbf{OsC_3P_4Re}$ (- - -) and $\mathbf{OsC_4P_4Re}$ (···).

assignment of a spin-forbidden d−d transition,[40] here the absorption bands are 1 or 2 orders of magnitude greater in intensity, which contradicts the assignment of a forbidden d−d transition in this system. The parent complex of this series of compounds, $Re(CO)_5Cl$, was known to luminescent from a d−d excited state.[40b] Upon replacement of two CO ligands with bipyridine or *o*-phenanthroline, the lowest excited state was reported as a metal-to-ligand charge transfer (MLCT) state.[40,42a] The polyphosphine ligands used in this study, similar to polypyridyl ligands, most likely possess low-lying ring and polyene π-antibonding orbitals capable of participation in charge transfer interactions. Hence, a metal-to-phosphine charge transfer state is assigned as the emitting excited state based on the literature study and the observed extinction coefficients.

The heterobimetallic compounds exhibited ^{1}MLCT bands similar to those observed for the corresponding Ru^{II} and Os^{II} monometallic complexes $\mathbf{MC_nP_4}$ (M = Ru, Os; n = 3, 4). The ^{1}MLCT bands for these heterobimetallic compounds occurred around the same region (430−440 nm) as the Re^I-based MLCT band, but with stronger extinction coefficients ($\epsilon \approx 10^3-10^4$ M^{-1} cm^{-1}). The Os^{II} complexes ($\mathbf{OsC_3P_4Re}$ and $\mathbf{OsC_4P_4Re}$) also exhibit an additional metal-to-ligand charge transfer band that was triplet in nature (^{3}MLCT). This ^{3}MLCT band occurred between 580 and 600 nm (Figure 6b) with extinction coefficients $\epsilon \approx 10^3$ M^{-1} cm^{-1}. This assignment is in agreement with our earlier observations in the corresponding mono- and homobimetallic Os^{II} complexes containing the same spacers with cumulenic bridges.[3,6] In addition, from a comparison of the extinction coefficients in the absorption spectra of the mono- and homobimetallic complexes with Re^I, Ru^{II}, or Os^{II} centers, the percentage of chromophores excited can be calculated at different excitation wavelengths. It was determined that the Re^I-based ^{1}MLCT band is responsible for ∼50% of the light absorption at the excitation wavelength of 350 nm, while use of light at 450 nm leads primarily to the excitation (∼80%) of the Ru^{II}- and Os^{II}-based chromophores. The consequences of these results will be made evident in the later discussion of energy transfer within this system.

Table 8. Photophysical Data for Re^I Complexes

compound	λ_{em},[a] nm	τ,[a] ns (±10%) Re based[e]	Ru based	Os based	$\Phi^{a,b}$ (×10^{-3}) (±10%)	k_r,[c] s^{-1}	k_{nr},[d] s^{-1}
$\mathbf{ReC_2P_2e}$	480	2.1			2.28	1.1×10^6	4.8×10^8
$\mathbf{ReC_3P_4}$	480	3.3			4.42	1.3×10^6	3.0×10^8
$\mathbf{ReC_4P_4}$	530	6.8			1.83	2.7×10^5	1.5×10^8
$\mathbf{ReC_3P_4Re}$	480	4.5			0.53	1.1×10^5	2.2×10^8
$\mathbf{ReC_4P_4Re}$	530	8.9			0.32	3.6×10^4	1.1×10^8
$\mathbf{RuC_3P_4Re}$	600	*f*	12.4		2.24	1.8×10^5	8.0×10^7
$\mathbf{RuC_4P_4Re}$	605	*f*	10.3		6.51	6.3×10^5	9.6×10^7
$\mathbf{OsC_3P_4Re}$	580	1.1		983	65.06	6.6×10^4	9.5×10^5
$\mathbf{OsC_4P_4Re}$	610	*f*		760	41.00	5.3×10^4	1.3×10^6

[a] λ_{ex} = 420 nm for the mono- and homobimetallic complexes and 450 nm for the heterobimetallic complexes, in acetonitrile at 295 K. All solution samples were treated three times with freeze−pump−thaw cycles before the measurements of emission and quantum yields. Luminescence lifetimes are obtained from the least-squares fit of single-exponential decay. [b] Φ_{em} vs $Ru(bpy)_3(PF_6)_2$ (Φ_{em} = 0.062). [c] $k_r = \Phi_{em}\tau^{-1}$. [d] $k_{nr} = \tau^{-1} - k_r$. [e] Measurements were performed on the phase-modulated fluorescence system (500 ps to 200 ns). [f] Lifetime of the quenched Re^I excited state is shorter than the detection limit of the system.

The excited-state emission and lifetime data are collected in Table 8 along with the resulting calculated values for the observed quantum yield, Φ, and the radiative and nonradiative decay rate constants, k_r and k_{nr}, respectively. The monometallic complexes $\mathbf{ReC_2P_2e}$, $\mathbf{ReC_3P_4}$, and $\mathbf{ReC_4P_4}$ were found to exhibit weak luminescence at 480, 480, and 530 nm, respectively. For comparison, the emission maximum for the pentacarbonyl starting material, $Re(CO)_5Cl$, occurred at 500 nm.[40] The emission of $\mathbf{ReC_4P_4}$ was slightly red shifted with respect to the other two monometallic complexes with shorter spacers and the $Re(CO)_5Cl$ starting material. This observation is a result of the increased σ-donating ability of the longer spacer, as evidenced by the previously reported electrochemical and XPS studies of the Ru^{II} and Os^{II} complexes,[3a] which appears to decrease the gap between the ground state and the MLCT state. The same trend was observed for the two homobimetallic species, $\mathbf{ReC_3P_4Re}$ and $\mathbf{ReC_4P_4Re}$, at 480 and 530 nm, respectively.

Regarding the lifetimes of the new complexes with the Re^I center, it was observed that as the length of the cumulenic ligand was increased for the monometallic species, the lifetime of the Re^I exited-state emission also slightly increased: 2.1 ns for $\mathbf{ReC_2P_2e}$, 3.3 ns for $\mathbf{ReC_3P_4}$, and 6.8 ns for $\mathbf{ReC_4P_4}$. The same trend was also witnessed for the two homobimetallic species, $\mathbf{ReC_3P_4Re}$ and $\mathbf{ReC_4P_4Re}$, 4.5 and 10.9 ns, respectively. As previously discussed, the longer the rigid cumulenic backbone of the spacer becomes, the more σ-donation occurs from the spacer to the metal termini, causing a decrease in the triplet energy level. Such lowering of the MLCT state may inhibit the mixing with other higher energy excited states and results in the slight prolongation of the triplet-state lifetime. For heterometallic systems, the lifetimes from Re^I excited state were not

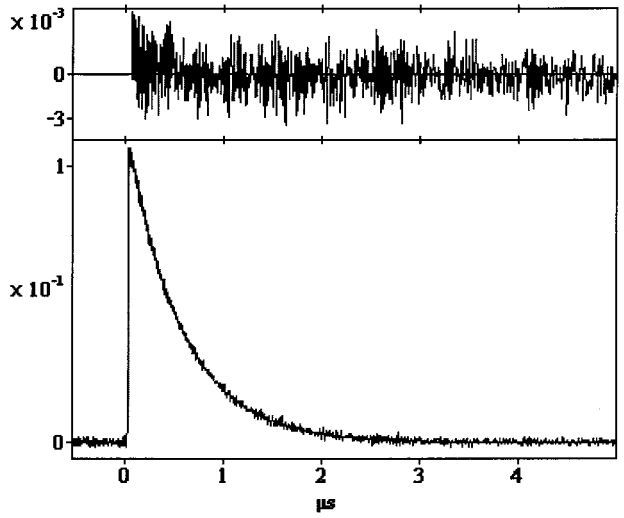

Figure 7. Representative decay trace and fit for **OsC_3P_4Re**.

measurable on our current setup, and only lifetimes of the Ru^{II} or Os^{II} chromophores were obtained and are listed in Table 8. A representative decay trace and fit for **OsC_3P_4Re** are shown in Figure 7. All of the emission decay traces fit to single-exponential decay curves, leading to the conclusion that the emissions are predominately from the Ru^{II}- or Os^{II}-based chromophores.

The quantum yields, Φ, were calculated from the steady-state emission measurements and referenced to a standard solution of $[Ru(bpy)_3][PF_6]_2$ ($\Phi = 0.062$ in acetonitrile).[14] The Os^{II}-containing heterometallic compounds exhibited the largest Φ (0.065 and 0.041), while those for the Re^{I} monometallic compounds were an order of magnitude smaller ($\sim 10^{-3}$). The Φ values of **ReC_3P_4Re** and **ReC_4P_4Re** were another order of magnitude smaller ($\sim 10^{-4}$) than the corresponding monometallic complexes **ReC_3P_4** and **ReC_4P_4**. The radiative decay rate constant, k_r, was calculated for each compound from the emission quantum yield and the lifetime of the emitting MLCT state ($k_r = \Phi/\tau$). The highly emissive Os^{II}-containing compounds, however, exhibited the smallest k_r ($\sim 10^4$) with respect to the Re^{I}-only compounds ($\sim 10^5 - 10^6$), while also displaying the smallest nonradiative decay constant ($k_{nr} = 1/\tau - k_r$) ($\sim 10^6$). While the low k_{nr} is in agreement with the high Φ, the relatively low k_r is in contradiction with what is expected from more emissive compounds. For complexes with a higher degree of electronic coupling across the bridging units, there is also the possibility of the presence of low-lying, unoccupied orbitals, including the low-energy ligand-based excited states.[43,44] Therefore, the low observed k_r may be a result of the deactivation of the emitting ^{3}MLCT state by mixing with low lying nonemitting ligand-based excited states (i.e., $p\pi^*(L)$). Another possibility is the rapid relaxation of the ^{1}MLCT state to the ground state before a substantial amount of intersystem crossing can occur to afford the emitting ^{3}MLCT state. The former would explain how a k_r value could be decreased without increasing k_{nr} of the same system. The Re^{I}-only complexes have the greatest k_{nr}, which is in agreement with the low Φ values. Apparently, the

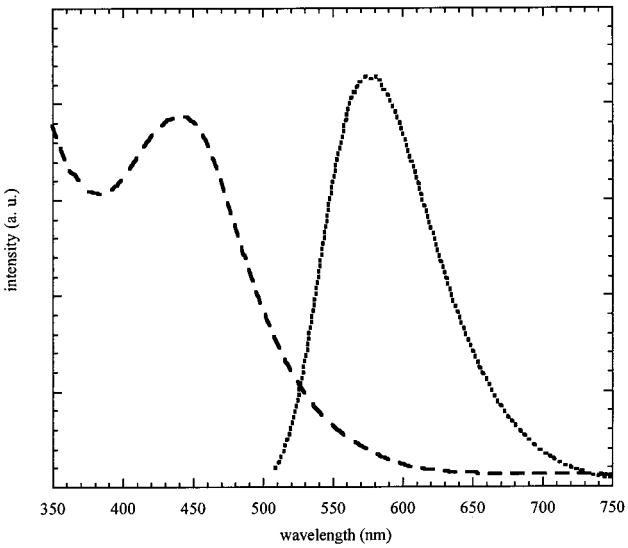

Figure 8. Representative comparison of the absorption spectrum (- - -) with the emission spectrum (···) of the Os^{II} heterobimetallic complex **OsC_3P_4Re**.

Re^{I}-based chromophores in this system are not as efficient as the Os^{II}- and Ru^{II}-based ones. However, even though the heterometallic compounds in this study have relatively low k_r values, such values are still an order of magnitude greater than the corresponding monometallic complexes **MC_nP_4** (M = Ru, Os; $n = 3, 4$) without the Re^{I} pentacarbonyl unit.

Energy Transfer. The rate constant of energy transfer could not be calculated for the four heterobimetallic complexes with Re^{I}/Ru^{II} and Re^{I}/Os^{II} donor/acceptor pairs due to the inability to determine the lifetime of the Re^{I} donor in heterometallic systems. Therefore, the mechanism by which any possible energy transfer process occurs could not be identified. However, these complexes exhibited excited-state behavior that was indicative of an efficient energy transfer. The emission maxima for the four heterobimetallic complexes were found between 580 and 610 nm (Table 8), which were assigned as Ru^{II}- and Os^{II}-centered on the basis of comparison of their luminescence properties with the corresponding monometallic model complexes with the same spacers.[3] These emission maxima are red-shifted significantly from the Re^{I}-based mono- and homobimetallic complexes and occur in the region associated with the Ru^{II} and Os^{II} ^{3}MLCT energies. The fact that no Re^{I}-based emission is detected is a possible consequence of the energy transfer from the higher MLCT Re^{I} excited state to the lower Ru^{II}- and Os^{II}-based excited states. A representative comparison of the absorption spectrum with the emission spectrum of the heterobimetallic **OsC_3P_4Re** is shown in Figure 8. It is also noted that the observed emission maxima from the Re^{I} centers occurred in the same region and overlapped with the absorption energy of the corresponding Ru^{II} and Os^{II} monometallic complexes (440−460 nm and 550−615 nm, respectively). In addition, the driving force, $\Delta G°$, of such energy transfer can be estimated for the Re^{I}/Ru^{II} and Re^{I}/Os^{II} donor/acceptor combinations. By calculating the difference in the spectroscopic energies of the donor and acceptor using the equation $\Delta G° = \lambda_{em}(\text{donor}) - \lambda_{em}(\text{acceptor})$,[39,44] the driving force was found to be exothermic for the four heterobimetallic complexes. The values thus obtained were −0.36 eV for **RuC_3P_4Re**, −0.44 eV for **OsC_3P_4Re**, −0.25 eV for **RuC_4P_4Re**, and −0.46 eV for **OsC_4P_4Re**.

In the aforementioned electronic absorption study, it was determined that at 350 nm the Re^{I} center absorbs *ca*. 50% of

(43) Baba, A. I.; Ensley, H. E.; Schmehl, R. H. *Inorg. Chem.* **1995**, *34*, 1198−1207.

(44) (a) Sauvage, J.-P.; Colin, J.-P.; Chambron, J.-C.; Guillercz, S.; Cudret, C.; Balzani, V.; Barigelletti, F.; De Cola, L.; Flamigni, L. *Chem. Rev.* **1994**, *94*, 993. (b) Barigelletti, F.; Flamigni, L.; Balzani, V.; Collin, J.-P.; Sauvage, J.-P.; Sour, A.; Constable, E. C.; Thompson, A. M. W. C. *J. Am. Chem. Soc.* **1994**, *116*, 7692. (c) Schlicke, B.; Belser, P.; De Cola, L.; Sabbioni, E.; Balzani, V. *J. Am. Chem. Soc.* **1999**, *121*, 4207.

the incident light energy, while at 450 nm the Re^{I} chromophore absorbs only *ca*. 20%. Excitation using both wavelengths of heterobimetallic complexes led to practically identical quantum yield results (*ca*. 1% difference). This result suggests that irrespective of which chromophore absorbs the excitation radiation, the emission is occurring from a single metal center (i.e., Os(II)* or Ru(II)*) in each heterometallic complex with $\mathbf{C_nP_4}$ ($n = 3, 4$) spacers.

Concluding Remarks

Several different characterization techniques were successfully employed in the identification and study of the multicomponent complexes with cumulenic spacers. The FAB mass spectral technique, as a relatively soft ionization process, afforded the characterization of the fragmentation and isotope patterns as well as the identity of the species. While different fragmentation did occur, the loss of the counterion PF_6, the linkage component PPh_2, and the ligands Cl and CO were observed. The addition of oxygen atoms was also observed as a characteristic phenomenon in the FAB/MS analysis. Furthermore, single-crystal X-ray structure determination provides a comparison of the metal-to-metal distances and dihedral angles that exist between the odd- and even-numbered cumulenic spacers. The metal-to-metal distance for **ReC_4P_4Re** was found to be 1.33 Å longer than in **ReC_3P_4Re**. Due to the resulting four-membered ring upon complexation to the Re^{I} center, the ligand coordination angle for both complexes was much smaller than the ideal 120° expected for sp^2-hybridized carbons. In addition, the IR techniques have also been utilized to describe the electronic donating ability of the different cumulenic spacers in addition to confirming the local coordination environment described by X-ray crystal structure determination for the Re^{I} units.

The photophysical properties of these supramolecular complexes with rigid spacers were explored through the utilization of several spectroscopic techniques. The electronic absorption spectra characterized the effects of the substitution of the N-donor bpy ligands by the P-donor rigid spacers. The decrease in σ-donation from the P-donors with respect to the N-donors caused the destabilization of the MLCT excited state and the stabilization of the ground state, resulting in a blue shift to higher energies for these molecular complexes. A red shift was observed as the length of the spacer was increased resulting from the higher amount of π-electrons in the spacer, which gives rise to an increase in the σ-donation from the phosphine units.

Due to the weak and relatively short excited-state lifetimes of the Re^{I} components in the heterobimetallic complexes, the energy transfer rate constant could not be calculated and the mechanism by which any possible energy transfer occurs could not be identified. However, on the basis of their excited-state behavior, these complexes were found to be capable of energy transfer from the Re^{I} center to the Ru^{II} and Os^{II} centers. Only the Ru^{II}- and Os^{II}-based ^{3}MLCT emissions were detected, and excitation at different wavelengths, where a different percentage of different metal-based chromophores were excited, resulted in identical quantum yield values. These observations are indicative of a highly efficient energy transfer process across the polyphosphine spacers with cumulenic carbon chains.

Acknowledgment. This work was supported by the National Science Foundation CAREER award (CHE-9733546). We thank Dr. John Greaves (UCI Mass Spectral Laboratory) for his assistance in the FAB/MS analysis.

Supporting Information Available: Atomic coordinates, thermal parameters, and bond lengths and angles have been deposited at the Cambridge Crystallographic Data Center (CCDC). Any request to the CCDC for this material should quote the full literature citation and the reference number 146268 for **ReC_3P_4Re** and 146269 for **ReC_4P_4Re**. Tables listing detailed crystallographic data, atomic parameters, and bond lengths and bond angles. This material is available free of charge via the Internet at http://pubs.acs.org.

IC0006910